BROCK UNIVERSITY LIBRARY
3 9157 00903119 9

Order and membrane organization in chlorhexidine–lipid mixtures

by

Sara Sadeghi

A THESIS SUBMITTED IN PARTIAL FULFILMENT OF
THE REQUIREMENTS FOR THE DEGREE OF

MASTER OF SCIENCE

in

The Faculty of Mathematics and Sciences

Department of Physics

BROCK UNIVERSITY

October 12, 2007

2006 © Sara Sadeghi

Abstract

Formulations of a general bactericidal agent, chlorhexidine, mixed with a phospholipid at different concentrations are investigated using ^{2}H NMR spectroscopy on a chain-deuterated lipid analog. Lipid-chlorhexidine formulation is known to release the drug into an aqueous medium slowly, maintaining a comparable concentration of the drug for up to four times longer than a direct aqueous solution. The NMR data does not support the proposed liposomal entrapment of chlorhexidine in lipid compartments. Complex thermal history of the lipid-chlorhexidine preparations is investigated in detail.

In preparation for a counterpart measurement, using ^{2}H NMR of deuterated chlorhexidine mixed with protonated lipid, the synthesis of a deuterated analog of chlorhexidine is performed.

Contents

Abstract ii

Contents iii

List of Tables v

List of Figures vi

Acknowledgements viii

1 Introduction 1

- 1.1 Lipids and membranes 1
  - 1.1.1 Lipids 1
  - 1.1.2 Organization of lipids in water 1
  - 1.1.3 Biological and model membranes 4
- 1.2 Liposomal drug delivery 7
- 1.3 Chlorhexidine 9
  - 1.3.1 Role in dental medication 11

2 ^{2}H NMR as a tool for studying lipid organization 14

- 2.1 NMR, the classical and quantum pictures 14
- 2.2 Relaxation 17
- 2.3 Spin-1 systems 18
- 2.4 Order parameter reports on molecular motions 19

2.5 Distribution functions and powder spectra . . . 21
2.6 DePakeing via Tikhonov regularization . . . 23

3 Synthesis of deuterated chlorhexidine . . . 26

4 Experimental results . . . 35
4.1 NMR spectroscopy . . . 36
4.2 Spectral moments . . . 38
4.3 ^{2}H NMR spectra . . . 38
4.4 T_{1z} and relaxation . . . 38
4.5 De-Pake-ing and order parameter profiles . . . 43

5 Concluding remarks . . . 58

Bibliography . . . 62

List of Tables

4.1 Thermal history of T_2^{qe} of the 3:1 sample 42
4.2 Thermal history of T_2^{qe} of 10:1 sample 44
4.3 T_{1z}^{ir} of the 3:1 sample 47
4.4 T_{1z}^{ir} of 10:1 sample 48

List of Figures

1.1 An illustration of different types of phospholipids 2

1.2 Common self-organized structures of lipids in aqueous environment 3

1.3 Schematic representation of a biological membrane 4

1.4 Phase transition from gel phase to liquid-crystalline phase 6

1.5 Different motions of phospholipids in a membrane 7

1.6 Time scales of lipid bilayer dynamics and measurement techniques 8

1.7 Different mechanisms of liposomal drug delivery 10

1.8 Deuterated Chlorhexidine 11

1.9 Effects of rinsing chlorhexidine as a mouth-wash on Plaque Index 12

1.10 Lipid-chlorhexidine mixtures provide better anti-bacterial action through a delayed release of the drug 13

2.1 Precession of the magnetic moment, the classical view 15

2.2 Zeeman splitting and quadrupolar shifting 16

2.3 Schematic figure of relaxation mechanism. Reproduced from [4] 17

2.4 Powder pattern 22

2.5 d_{54}-DMPC powder pattern at 35°C [13] 23

3.1 Synthesis of ^{14}C-labeled chlorhexidine as reported by Burns [5]. 27

3.2 First attempted synthesis of deuterated chlorhexidine. 28

3.3 Second attempted synthesis of deuterated chlorhexidine. 29

3.4 The chemical pathway used for the synthesis of deuterated chlorhexidine. . . 30

3.5 ^{1}H NMR spectrum of chlorhexidine deuterated in the saturated-chain methylenes. 34

4.1 1,2-dimyristoyl-d_{54}-glycero-3-phosphocholine (DMPC-d_{54}) Reproduced from `www.Avantilipids.com` 35

4.2 Representative ^{2}H NMR spectra for the $x = 3:1$ samples 39

4.3 Representative ^{2}H NMR spectra for the $x = 10:1$ samples 40

4.4 The temperature dependence of the second moments of the spectra for the $x = 3:1$ (top) and $x = 10:1$ (bottom) samples through the various heating/cooling runs 41

4.5 The temperature dependence of the T_2 times for the $x = 3:1$ (top) and $x = 10:1$ (bottom) samples from Tables 4.1 and 4.2. 45

4.6 A typical fit to a two-exponential decay curve for T_{1z} times, here for the $x = 3:1$ at 25°C. 46

4.7 Extracting the distribution of anisotropy from the d_{54}-DMPC:Ch (10:1) powder spectrum 49

4.8 Depaked intensity and order parameter profile for 10:1 sample at 15° 50

4.9 Depaked intensity and order parameter profile for 10:1 sample at 35° 51

4.10 Depaked intensity and order parameter profile for 10:1 sample at 60° 52

4.11 Depaked intensity and order parameter profile for 3:1 sample at 15° 53

4.12 Depaked intensity and order parameter profile for 3:1 sample at 35° 54

4.13 Depaked intensity and order parameter profile for 3:1 sample at 60° 55

4.14 Order parameter of pure DMPC-d54, and lipid:chlorhexidine mixtures with ratios 10:1 and 3:1 56

5.1 Molecular models illustrating the possibility of chlorhexidine incorporation into the DMPC bilayer 60

5.2 Molecular models illustrating the aromatics of chlorhexidine located near phosphate group of DMPC 60

Acknowledgements

I would like to thank my supervisor Prof. E. Sternin, who has been helping me during my study at Brock. Also I like to say thanks to Prof. F. Razavi and Prof. B. Mitrovic, members of my committee, and Prof. T. Hudlicky and Dr. M. Moser from the Chemistry Department who supervised me during the synthesis of deuterated analog of chlorhexidine. I will never forget helpful attitude of all other members of the Physics Department. Also, I want to say thank you to all of my friends at Brock University, and especially to R. Carrol and I. Komljenovic who helped me with the editing of my thesis.

In addition my special thanks are for my parents and my brother who have been supporting me from over the seas.

Chapter 1

Introduction

1.1 Lipids and membranes

1.1.1 Lipids

Lipids are chemical compounds readily soluble in organic solvents and essentially insoluble in water. Lipids typically contain two structural regions, a hydrophilic and a hydrophobic one; for example fatty acids have polar headgroups which are hydrophilic due to an unshared electron, and hydrocarbon chains which are hydrophobic. Fatty acids, and fatty-acid-chain-containing phospholipids are classified according to the structure of these hydrocarbon chains: these can be saturated (all carbon-carbon bonds are single bonds), unsaturated (some double bonds between carbons), or contain complex side groups. The most common lipids which make up most animal cell membranes are called glycerophospholipids, also known as glycerol phosphatides or phosphoglycerides. These phospholipids consist of a glycerol backbone, two fatty-acid chains, and a phosphate group which may be attached to a variety of headgroups. An illustration of different types of phospholipids is shown in Fig.1.1.

1.1.2 Organization of lipids in water

Large assemblies of amphiphilic phospholipid molecules tend to self-organize when placed in an aqueous medium so as to minimize the free energy of interaction with water. To achieve this, the hydrophilic head-groups are turned toward the aqueous environment and

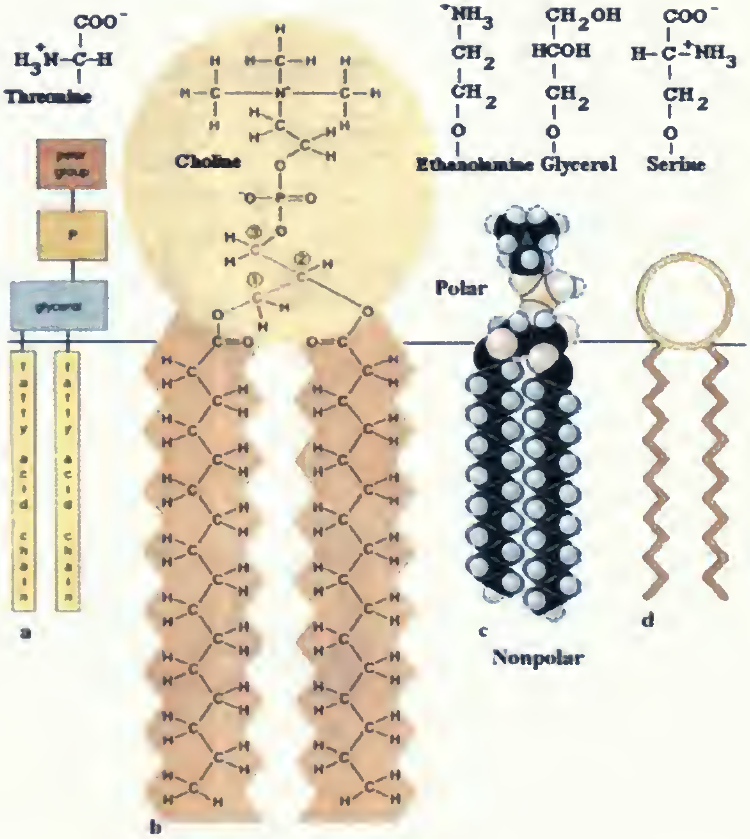
Threonine
Choline
Ethanolamine
Glycerol
Serine
polar group
P
glycerol
fatty acid chain
fatty acid chain
Polar
Nonpolar
a
b
c
d

Figure 1.1: **An illustration of different types of phospholipids (a)** A schematic representation of a phospholipid molecule. **(b)** Chemical structure of a phosphotidylcholine. **(c)** The space-filling model. **(d)** A structural illustration. Some common headgroups are shown near the top. Reproduced from [40]

the fatty acids are facing away from it. The nature of observed structural arrangements depend on concentration of lipids in water, pH, temperature, *etc.* There are many possibilities; some of the common structures are shown in Fig.1.2. According to Lipowsky [18], at

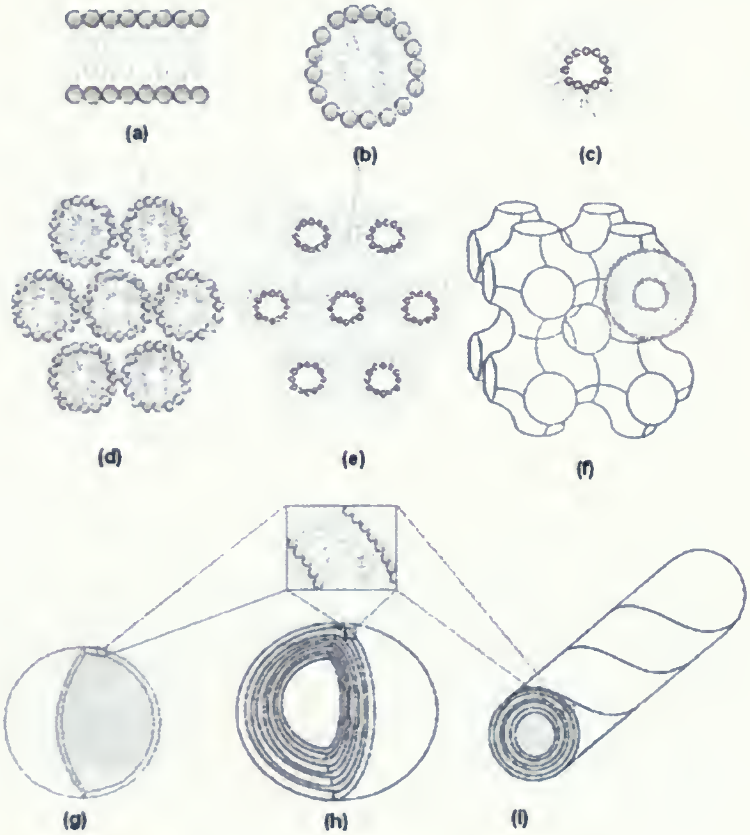

Figure 1.2: **Common self-organized structures of lipids in aqueous environment.** **(a)** bilayer; **(b)** micellar; **(c)** inverted micellar; **(d)** hexagonal; **(e)** inverted hexagonal; **(f)** cubic; **(g)** liposomal; **(h)** multilamellar vesicular (MLV); **(i)** tubular. Reproduced from [40]

low concentration in water the lipid molecules form micelles and vesicles at most temperatures. The temperature-concentration phase diagram typically also contains a region where the amphiphilic molecules are aggregated into cylindrical micelles. This phase undergoes a transition to a lamellar phase at higher lipid concentrations. Ordered cubic phase sometimes melts into a bicontinuous sponge phase which has no long-range translational order. Bilayers usually self-organize into liposomes or multilamellar vesicles (MLVs). In liposomes, aqueous solution is entrapped inside lipid compartments. A group of bilayers with an onion-like

structure make up MLVs; a single bilayer entrapping a volume of water is referred to as a unilamellar vesicle (ULV).

1.1.3 Biological and model membranes

Biomembrane is a semi-permeable barrier that separates the inside of a cell from its outside [39]. Cell membranes control the transport in and out of the entire cell or in and out of sub-cellular domains, depending on the size, charge, or other chemical properties of ions and molecules in the medium. General organization of a biological membrane is illustrated in Fig.1.3. The major components of cell membranes are lipids and proteins, making up between 20% to 80% of the dry weight of a typical biological membrane [12]. Model membranes containing only glycerophospholipids are well-suited to studying biological membranes as they share many physical similarities with their biological counterparts. Depending on the tem-

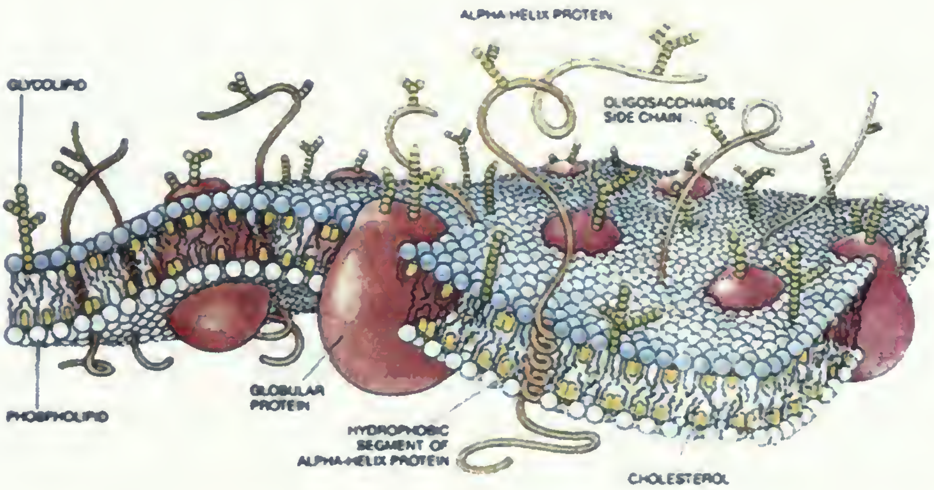
ALPHA HELIX PROTEIN
GLYCOLIPID
OLIGOSACCHARIDE SIDE CHAIN
GLOBULAR PROTEIN
PHOSPHOLIPID
HYDROPHOBIC SEGMENT OF ALPHA-HELIX PROTEIN
CHOLESTEROL

Figure 1.3: **Schematic representation of a biological membrane.** Phospholipids form the bilayer that is the main structural component of biological membranes. Glycolipids, cholesterol, trans-membrane proteins (typically, their α-helix segments), globular proteins, *etc.* may also be embedded in the biomembrane. Reproduced from `www.wikipedia.org`.

perature, model membranes may exhibit different structural phases, and varying degrees of molecular re-orientational motion. Usually at low temperature lipids organize into bilayers where the individual lipid molecules tend to be fairly ordered; this is referred to as the gel phase. At higher temperatures, lipid bilayers "melt" into a liquid-crystalline phase, where the bilayer organization is maintained, but the individual lipid molecules are relatively free to move, both translationally along the surface of the bilayer and rotationally about their long axes that tend to be oriented along the normal to the bilayer.

The differences between gel and liquid-crystalline phases are illustrated in Fig.1.4. The individual lipid molecules are seen to be more "ordered" in the gel phase, assuming mostly the "all-trans" conformational state; as a result, lipid bilayers tend to have greater thickness and a lower area per lipid molecule in the gel phase. Chain-melting phase transition temperature (T_M) depends on factors like chain length, degree of unsaturation, and head group composition. Longer carbon chains and saturated chains have higher T_M [14]. For example, for the same phosphatidylcholine headgroup, T_M is reported to be 23°C, 79°C, and -53°C for 14:0[1] (DMPC), 22:0[2] and 18:2 [3], respectively. Here, the first number is the carbon chain length, and the second is the number of unsaturated carbon–carbon bonds in each chain.

A variety of molecular motions exists in phospholipid bilayers, covering a broad range of time scales: flexing of the the carbon-carbon bonds (sometimes called trans-gauche isomerization, $\leq 10^{-10}$s), rapid re-orientation about the long axis of the phospholipid molecule (typically itself oriented close to the bilayer normal, 10^{-8}–10^{-9}s), transverse lateral diffusion within monolayers (10^{-6}–10^{-7}s), or a 'flip-flop' exchange of phospholipid molecules across the two sheets of a bilayer (10^{2}–10^{6}s), as illustrated in Fig.1.5. All of these motions become faster at higher temperature; in addition, structural re-organizations or changes in the packing of the phospholipid molecules may cause certain motions to be dramatically enhanced or suppressed.

---

[1] 1,2-dimyristoyl-*sn*-glycero-3-phosphocholine

[2] 1,2-dibehenoyl-*sn*-glycero-3-phosphocholine

[3] 1,2-dilinoleoyl-*sn*-glycero-3-phosphocholine

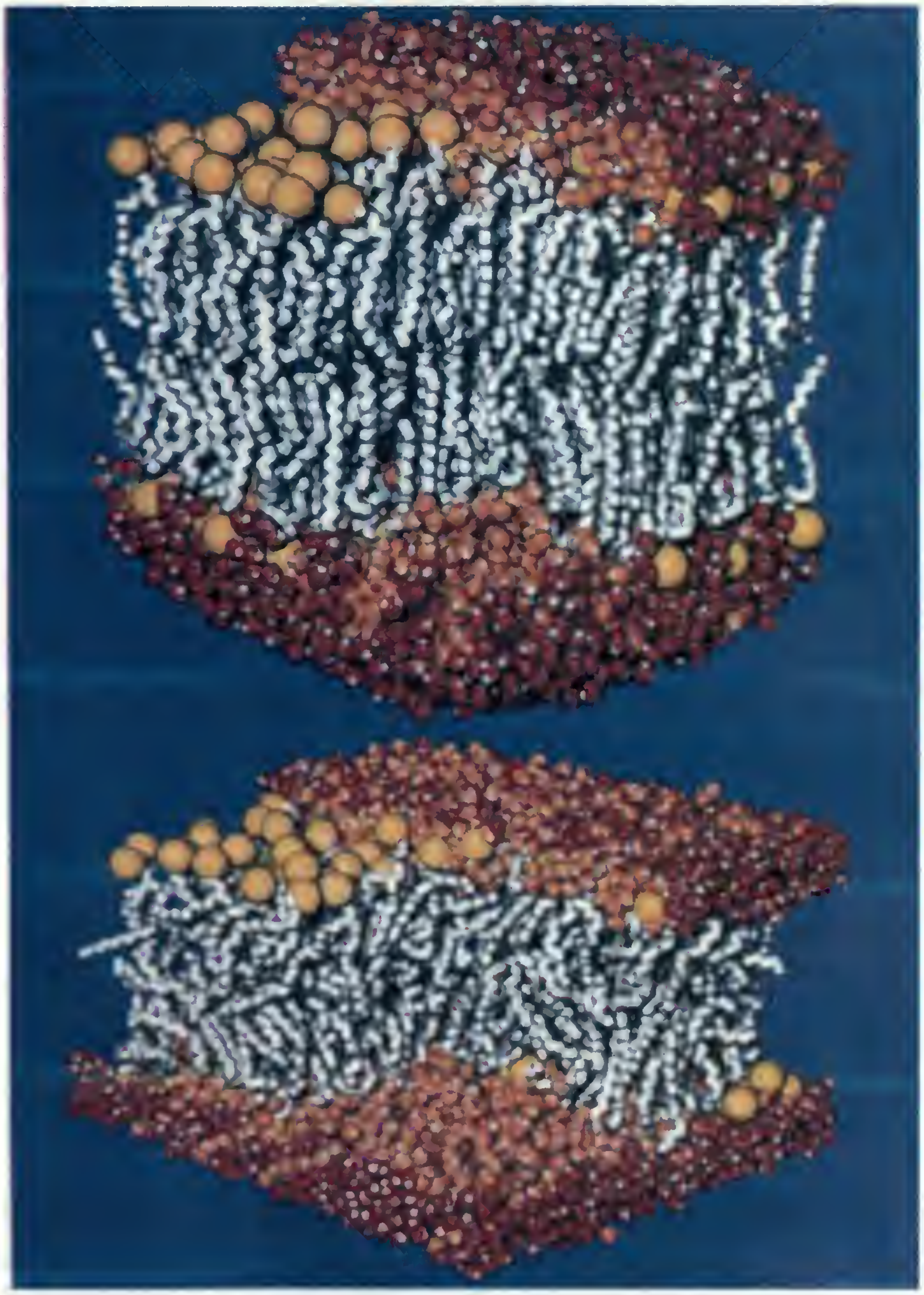

Figure 1.4: **Phase transition from gel to liquid-crystalline phase**, Reproduced from [14]

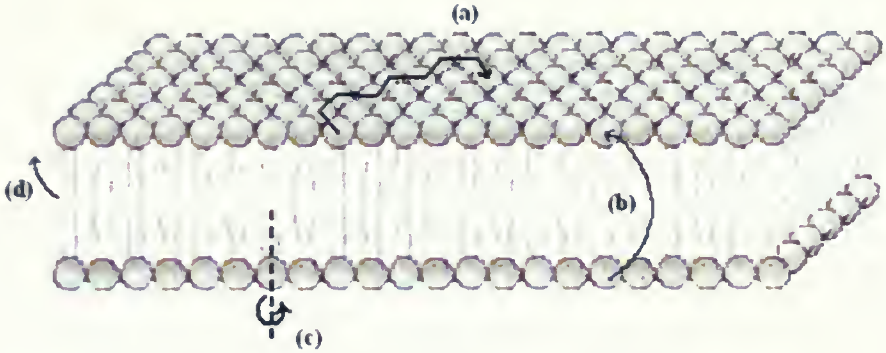

Figure 1.5: **Different motions of phospholipids in a membrane:** **(a)** lateral diffusion; **(b)** flip-flop or transverse diffusion; **(c)** re-orientation about the molecular axis; **(d)** trans-gauche isomerization [21]

The range of time scales and of the experimental techniques that are capable of accessing them is summarized in Fig. 1.6. NMR occupies a unique position among the experimental techniques in being able to access the broadest range of time scales, and thus it has had a considerable success in investigating structure and dynamics of biomembrane systems. In a given NMR experiment, interactions that are modulated by molecular motions are seen as *averages* if the motions are fast, and as *superpositions* of a series of 'snapshots' if the motions are slow on the NMR time scale, determined by the inverse of the width of the observed NMR spectra. For ^{2}H NMR in biomembranes, this time scale is 10^{-4}–10^{-5}s.

1.2 Liposomal drug delivery

Among all self-organized structures of lipids in water, liposomes offer a unique promise of encapsulating water-soluble drugs for targeted delivery through an aqueous medium such as blood or saliva. Drugs entrapped inside liposomes are protected from early release and possible degradation within the body. This property of liposomes can help reduce dosage and extend the effect of the drug [32]. The rate of release depends on the drug properties, liposome composition, pH of the medium, and other factors[1].

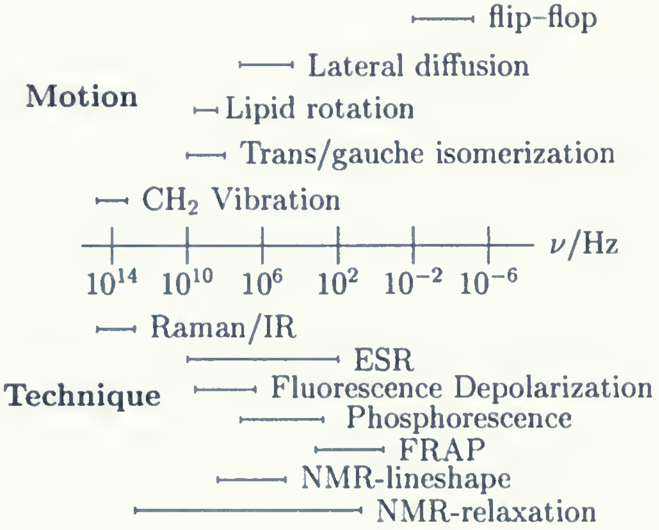
flip–flop
Lateral diffusion
Motion
Lipid rotation
Trans/gauche isomerization
CH₂ Vibration
ν/Hz
10¹⁴ 10¹⁰ 10⁶ 10² 10⁻² 10⁻⁶
Raman/IR
ESR
Technique
Fluorescence Depolarization
Phosphorescence
FRAP
NMR-lineshape
NMR-relaxation

Figure 1.6: **Time scales of lipid bilayer dynamics and measurement techniques for their investigation.** *Trans-gauche isomerization* increases along the tail at longer distances from the headgroup. *Rotation*, also known as rotational diffusion is the net movement about the long axis of the phospholipid. *Lateral diffusion* is the rapid exchange of place with neighbouring phospholipids. *Flip-flop* is the exchange of phospholipids between the monolayers, an extremely rare spontaneous event. In living biological systems this is a protein-mediated process. Reproduced from [6]

Liposomes can release their contents in one of the following four ways: adsorption, endocytosis, lipid exchange, or fusion [22, 41]. During adsorption process the contents of liposomes are not released directly into the cell; they first leak slowly into the extracellular fluid and then are adsorbed across the membrane. During endocytosis, the cell is engulfing entire liposomes with its cell membrane. In this way, the substances that are polar or too big to pass through the membrane directly can be delivered to the interior of the cell. During lipid exchange process, the individual lipid molecules transfer from the liposome to the plasma membrane; since the contents of the interior are not transferred to the cell, only drugs associated with the lipids themselves may be delivered in this way. Fusion is the intercalation of the outer membrane of the liposome into the cell membrane with concomitant release of the aqueous contents or the liposome directly into the cell's cytoplasm. The four possibilities are illustrated in Fig.1.7.

1.3 Chlorhexidine

Chlorhexidine belongs to a class of compounds called diguanides. Many of these chemicals are known to possess both bacteriostatic and bactericidal properties [7]. Chlorhexidine is probably the most common of diguanides, with outstanding antibacterial properties. Its structure is shown in Fig.1.8; like all diguanides it contains a chain of carbons in the middle of the molecule.[4] Chlorhexidine first was synthesized by Rose and Swain [26] and through the last 50 years it has been used as a topical bactericide for skin infections, wounds, burns, in obstetrics and for bladder irrigation [5]. Also it has been used to combat dental plaque [15]. Even at high dilution chlorhexidine maintains a significant antibacterial activity.

---

[4] A chain-deuterated analogue is shown in Fig.1.8, see Chapter 3 for details

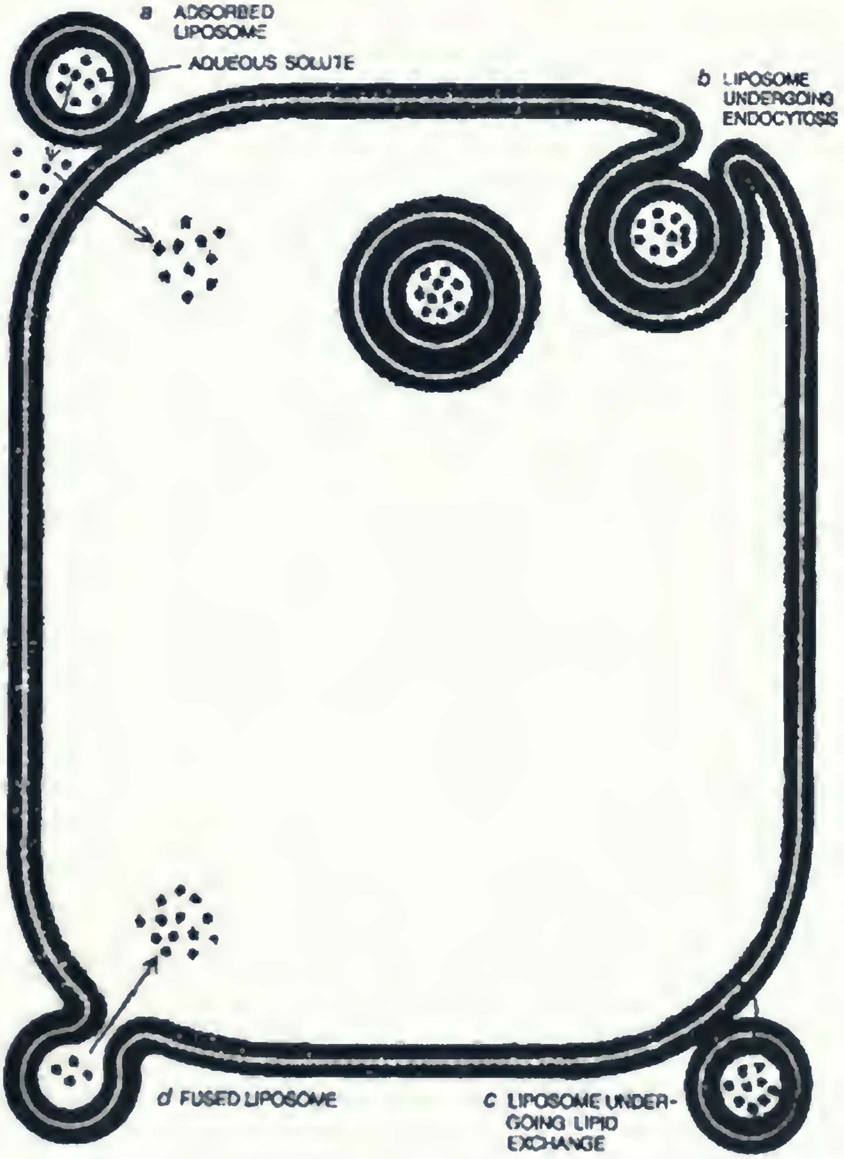
a ADSORBED LIPOSOME
AQUEOUS SOLUTE
b LIPOSOME UNDERGOING ENDOCYTOSIS
d FUSED LIPOSOME
c LIPOSOME UNDER-GOING LIPID EXCHANGE

Figure 1.7: **Different mechanisms of liposomal drug delivery**: **(a)** adsorption, **(b)** endocytosis, **(c)** lipid exchange, **(d)** fusion. Reproduced from [22].

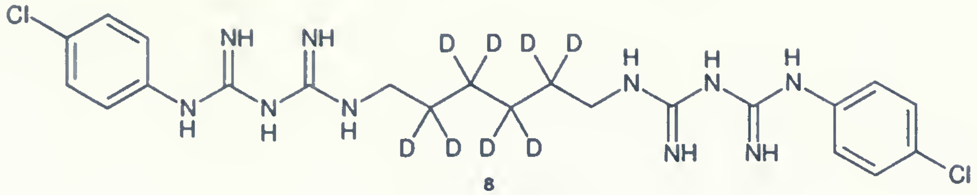

8

Chlorhexidine

Figure 1.8: Deuterated Chlorhexidine

1.3.1 Role in dental medication

As reported in 1970 by Harald Löe and C. Rindom Schiött [19], rinsing twice daily with 0.2% chlorhexidine gluconate solution resulted in the prevention of plaque formation on all tooth surfaces; no gingival changes occurred. When the subjects of the study stopped rinsing, but continued no-oral-hygiene program, the plaque and gingival index increased at rate closely resembling that of the non-rinsing control series Fig.1.9

Recently, mixtures of chlorhexidine with a variety of lipids has been reported to provide a superior anti-bacterial action, through a delayed release of the drug out of a drug-lipid (DPPC+CHG) formulation [20]. Fig. 1.10 shows that the measured bacterial counts mirror the kinetics of chlorhexidine concentration. The arrows in the upper frame of Fig. 1.10 are used to illustrate how the lipid-chlorhexidine formulation provides comparable concentration of the drug for up to four times longer than a direct aqueous solution. Entrapment of chlorhexidine in lipid compartments (liposomes?) has been proposed as the likely mechanism, however direct observation of lipid morphology has not been performed. This motivated the present work.

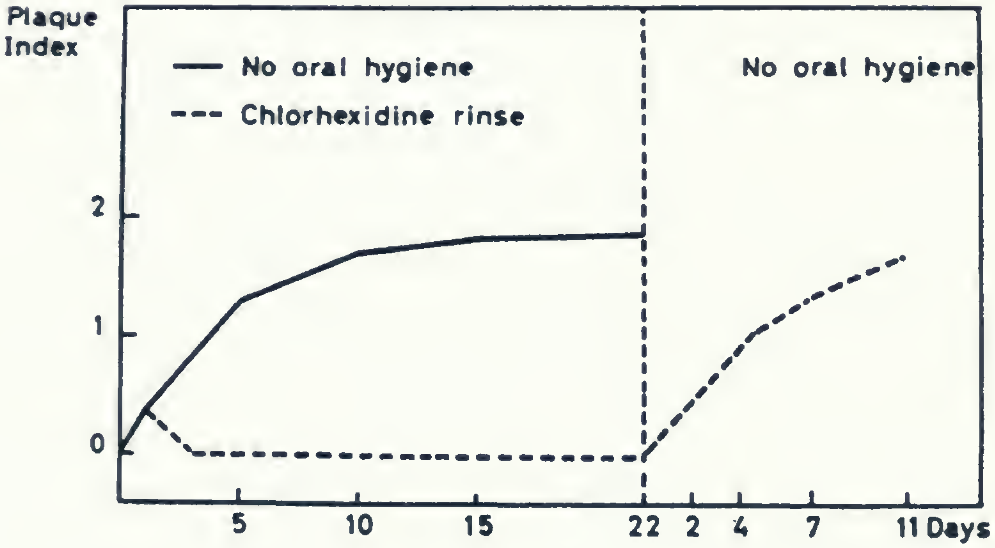

Figure 1.9: **Effects of rinsing chlorhexidine as a mouth-wash on Plaque Index.** Mean Plaque Index scores of four individuals during a period of 22 days without active oral hygiene (continuous line). The broken line designates the Plaque Index scores of the same subjects when active measures were substituted with two daily rinses with 0.2% chlorhexidine gluconate for 22 days, and when they ceased rinsing and subsequently continued on a no-oral-hygiene regime for 11 days. Reproduced from [19]

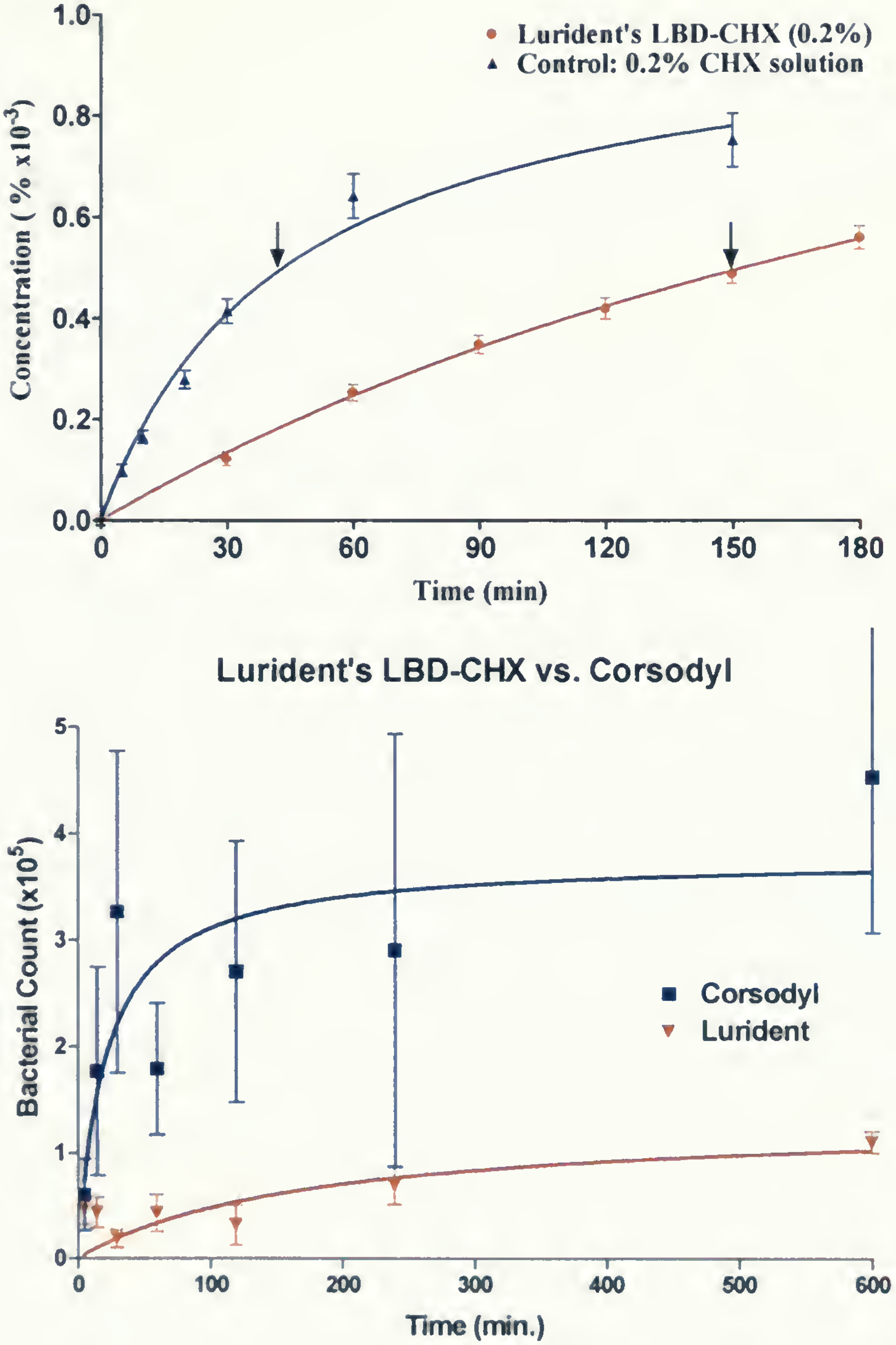

Figure 1.10: **Lipid-chlorhexidine mixtures provide better anti-bacterial action through a delayed release of the drug.** Note how the measured bacterial counts mirror the kinetics of chlorhexidine concentration. Reproduced from [20]

Chapter 2

^{2}H NMR as a tool for studying lipid organization

2.1 NMR, the classical and quantum pictures

Magnetic moment $\vec{\mu}$ of a nucleus is related to its intrinsic spin angular momentum, $\vec{S}$, through

$$\vec{\mu} = \gamma \vec{S} \tag{2.1}$$

where γ is the gyromagnetic ratio. When placed into an external magnetic field $\vec{H}_0$, the nuclear magnetic moments interact with the field, and the time evolution of the net magnetization vector

$$\vec{M} = \sum_i \vec{\mu}_i \tag{2.2}$$

is governed by

$$\frac{d\vec{M}}{dt} = \gamma \vec{M} \times \vec{H}_0 \quad . \tag{2.3}$$

The solution of the above equation is well-known, it is the classical precession of the magnetization vector about the field, at a precession frequency

$$\omega_0 = -\gamma H_0 \quad , \tag{2.4}$$

called the Larmor frequency. This precession is illustrated in Fig.2.1.

In a rotating frame of reference whose z-axis is directed along $\vec{H}_0$ while the frame is rotating about this axis at precisely the Larmor frequency, the effective static field is zero and the magnetization vector $\vec{M}$ appears stationary. When a weak transverse (*i.e.*, in the xy-plane) oscillating magnetic field $\vec{H}_1(t) \propto e^{-i\omega_0 t}$ is present in addition to the static magnetic

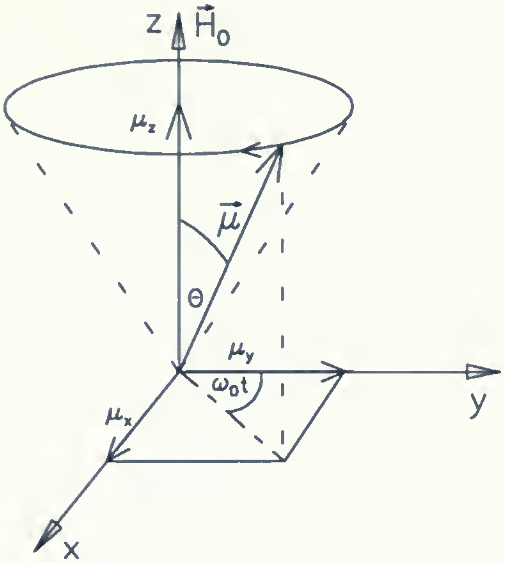

Figure 2.1: **Precession of the magnetic moment, the classical view**

field $\vec{H}_0$, this field, too, will appear static in the rotating reference frame, and will cause a precession of the magnetic moment, in the rotating frame, about the direction of the oscillating field. In a typical magnetic field of a few Tesla, the Larmor frequencies of most nuclei lie in the radio-frequency (rf) range. Thus, in Nuclear Magnetic Resonance (NMR) this transverse oscillating field is often referred to as the "rf field". If the rf field is applied for a total time t_{rf}, to net angle of rotation of the magnetization vector is

$$\theta = \gamma H_1 t_{rf} \quad . \tag{2.5}$$

When $\theta = \pi/2$, the magnetization is said to be rotated into the xy-plane, from its equilibrium orientation along the z-axis.

An equivalent description can be made from the quantum-mechanical point-of-view. A nucleus with spin S has $2S + 1$ possible eigenstates of the Hamiltonian

$$\mathcal{H} = -\gamma\hbar\hat{S}_z H_0 \tag{2.6}$$

where $\hat{S}_z$ is the z-component of the spin operator $\hat{S}$, with $\vec{H}_0$ providing the quantization along the z-direction. The energy levels of these states are separated by $\hbar\omega_0 = h\nu$ in the presence of an external magnetic field, where ω_0 is the Larmor frequency. This effect is

called Zeeman splitting, as illustrated in Fig.2.2. The populations of the Zeeman levels are determined by the Boltzmann factors, for a system in thermal equilibrium with a reservoir at temperature T,

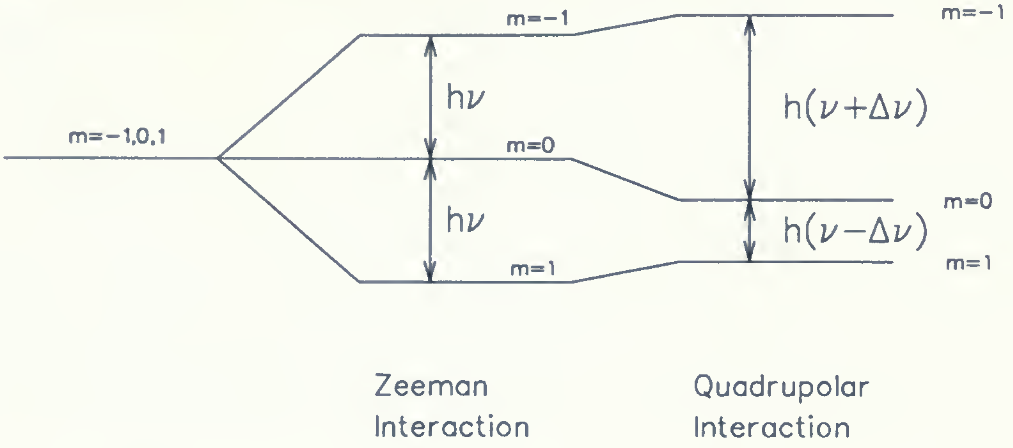

Figure 2.2: **Zeeman splitting and quadrupolar shifting**

Quadrupolar interaction shifts the Zeeman levels. Reproduced from [4]

$$\frac{N_i}{N_j} = e^{-(E_i-E_j)/k_BT} \quad . \tag{2.7}$$

A population difference between the Zeeman levels represents a coherence. For example, for a spin-$\frac{1}{2}$, there are two possible energy levels, representing the spin states along and against the external magnetic field, and the effective net magnetization (polarization) is proportional to the spin excess. A transverse oscillating field at the Larmor frequency ω_0, causes transitions between the energy levels separated by $\hbar\omega_0$. A resulting change in populations causes a change in the net magnetization of the system. For example, continuous irradiation with an oscillating field will equalize the populations of the two states and de-polarize the system, causing the net magnetization to approach zero. A coherent manipulation of the populations is also possible, for example a "180° rf pulse" will exchange the populations of the two states, causing a "flip" of the magnetization vector. For spins higher than $\frac{1}{2}$, similar description can be made, but in a space of states with dimensions higher than three [33].

2.2 Relaxation

Longitudinal NMR relaxation is the return of the magnetization to its equilibrium value after being perturbed by a transverse magnetic field H_1. The equilibrium magnetization direction is in the z-direction, along the external magnetic field. It is reached through an exchange of energy between the nuclear spin system and the surrounding molecular environment which is referred to as the lattice; this is the so-called spin-lattice relaxation. After a magnetization is perturbed from its equilibrium position, its z-component (longitudinal) tends to return to its equilibrium value with a time constant T_1.

Transverse relaxation is a form of loss of coherence due to irreversible spin-spin interactions, also called spin-spin relaxation. Transverse relaxation for a spin-$\frac{1}{2}$ system is illustrated in Fig.2.3 [4], shown in the frame of reference which rotates around H_0 at Larmor frequency.

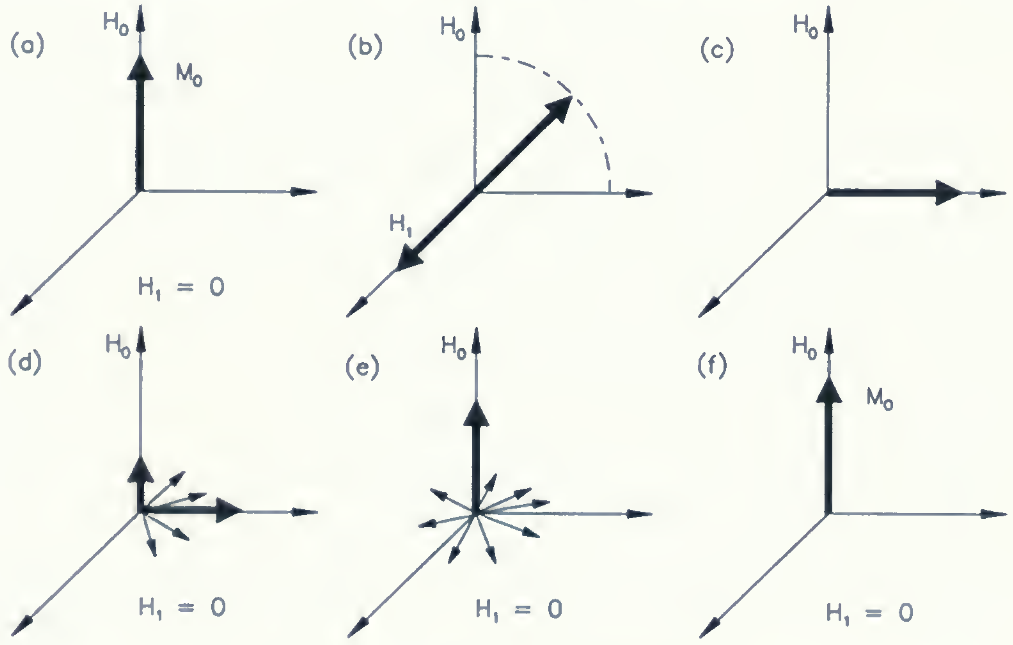

Figure 2.3: Schematic figure of relaxation mechanism. Reproduced from [4]

Initially, the magnetization vector is aligned with H_0, as in Fig.2.3(a). H_1, the transverse linearly-polarized magnetic field oscillating at the Larmor frequency, appears as a superposition of two field of opposite polarization, rotating at the Larmor frequency in the opposite

directions. In the rotating frame, one of these two fields appears static, while the other oscillates rapidly (at twice the Larmor frequency) and its influence is averaged out to zero. As seen in Fig.2.3(c), the static H_1 applied for an appropriate time duration rotates the magnetization into the xy-plane, and the magnetization vector begins to precess about H_0 after H_1 is turned off. Because of inhomogeneities in H_0, the Larmor frequencies of different nuclei vary, and the magnetization vector fans out, as in Fig.2.3(d). The decay of the transverse magnetization in the absence of the rf field H_1 is a free induction decay (FID). As local microscopic magnetic fields fluctuate randomly, they cause the loss of phase coherence as manifested in a decay in the strength of the net magnetization in the xy-plane. This decay is characterized by a time constant T_2.

Phenomenologically, these relaxation phenomena are described by the Bloch equations [2]:

$$\frac{dM_x}{dt} = \gamma(M_y H_0 - M_z H_1 \sin\omega_0 t) - \frac{M_x}{T_2} \quad (2.8)$$

$$\frac{dM_y}{dt} = -\gamma(M_x H_0 - M_z H_1 \cos\omega_0 t) - \frac{M_y}{T_2} \quad (2.9)$$

$$\frac{dM_z}{dt} = \gamma(M_x H_1 \sin\omega_0 t - M_y H_1 \cos\omega_0 t) - \frac{M_z - M_0}{T_1}. \quad (2.10)$$

The solutions, in a rotating reference frame, are well-known:

$$M_z(t) = M_z(0)e^{-t/T_{1z}} - M_0\left(1 - e^{-t/T_{1z}}\right) \quad (2.11)$$

$$M_x(t) = M_x(0)e^{-t/T_2} \quad (2.12)$$

$$M_y(t) = M_y(0)e^{-t/T_2}. \quad (2.13)$$

2.3 Spin-1 systems

Electric quadrupole moment which is possessed by spins greater than $\frac{1}{2}$ interacts with the electric field gradients (EFG) generated by the surrounding electron clouds. Although this effect is small relative to the Zeeman effect, it shifts the Zeeman levels slightly, as was seen in Fig.2.2. The greater the magnitude of the nuclear quadrupole moment and the stronger the electric field gradient, the bigger is the shift in energy levels.

Since EFG is due to the distribution of electronic charge, the principal axis system of the EFG tensor is a molecule-bound system. Associating the z-axis of the principal-axis reference frame of the EFG tensor with the direction of the chemical bond ($|V_{zz}| \gg |V_{xx}|, |V_{yy}|$), the quadrupolar interaction is described by the following Hamiltonian [31]:

$$\mathcal{H}_q = \frac{e^2qQ}{4S(2S-1)\hbar}\left[3\hat{S}_z{}^2 - \hat{S}^2 + \eta(\hat{S}_x{}^2 - \hat{S}_y{}^2)\right] \tag{2.14}$$

where eQ is the nuclear quadrupole moment, $V_{zz} = eq$, and η is the quadrupolar asymmetry parameter $\eta = \frac{V_{xx}-V_{yy}}{V_{zz}}$.

For an axially-symmetric field gradient, $V_{xx} = V_{yy}$ and therefore $\eta = 0$. In this case, for spin $S = 1$, the above Hamiltonian reduces to

$$\mathcal{H}_q = \frac{e^2qQ}{4S(2S-1)\hbar}\left(3\hat{S}_z{}^2 - 2\right) = \frac{\omega_q}{3}\left(3\hat{S}_z{}^2 - 2\right) \tag{2.15}$$

where $\omega_q = \frac{3}{4}\frac{e^2qQ}{\hbar}$ is called the quadrupolar frequency. For a C–D bond in a saturated hydrocarbon chain, $\omega_q \approx 2\pi \times 126$ kHz [10].

To transform the quadrupolar Hamiltonian (Eq. 2.14) from the principal-axis system of the EFG tensor to the laboratory frame where the observations are made, one can use the Wigner rotation matrices. It can be shown that the observed quadrupolar splitting is [9]:

$$\Delta\omega_q = 2\pi\Delta\nu = \omega_q\left[(3\cos^2\beta - 1) + \eta\cos 2\alpha \sin^2\beta\right] \tag{2.16}$$

where α and β are the Euler angles specifying the orientation of the principal-axis reference frame of the EFG tensor in the lab frame. It is clear that in axially symmetric cases, the anisotropy depends only on β, which is the angle between a particular carbon-deuterium bond and the direction of the external magnetic field H_0.

2.4 Order parameter reports on molecular motions

Molecular motions modulate $\beta = \beta(t)$ and thus influence the observed quadrupolar splitting. However, the anisotropy will be averaged out over those motions that are faster than the

interaction time frame, appearing as a motional narrowing of the signal. Axially symmetric environment in lipid samples is due to a rapid reorientational motion about the long axis of the lipid molecule. This axis is essentially normal to the lipid-water interface. Motional averaging projects the quadrupolar interactions of the individual C–D bonds onto bilayer normal.

On the other hand, the time modulation of the angle $\beta = \beta(t)$ caused by the motions that are slower than the interaction time frame will not average out, but will be seen as a superposition of signals from all β values. In biomembranes, with their rapid axially-symmetric reorientational motions about the bilayer normal, it makes sense to transform into the laboratory frame in two distinct steps: first, from the EFG frame associated with the C–D bond into the frame associated with the symmetry axis of the lipid molecule; and second, from this molecule-bound frame into the lab frame. Conventionally, the first transformation is described by Euler angles α' and β', and the second one by the Euler angles θ and ϕ. Time-average over rapidly-changing α' and β' yields a single scaling factor, called the orientational order parameter, S_{CD}, of the C–D bond,

$$S_{CD} = \frac{1}{2}\left\langle (3\cos^2\beta' - 1) + \eta\cos 2\alpha' \sin^2\beta' \right\rangle \tag{2.17}$$

where the averaging $\langle \ldots \rangle$ is over the rapid reorientational motions. In an axially symmetric case, $\eta = 0$ and the above reduces further to

$$S_{CD} = \frac{1}{2}\left\langle 3\cos^2\beta' - 1 \right\rangle. \tag{2.18}$$

Smaller values of S_{CD} correspond to more disorder, *i.e.* to rapid random reorientations of the C–D bonds. In fully isotropic liquids, $S_{CD} = 0$.

On the other hand, the average over all values of θ and ϕ is a superposition of many individual contributions, or a powder average:

$$\Delta\omega_q = \omega_q S_{CD} \left\langle 3\cos^2\theta - 1 \right\rangle \tag{2.19}$$

where the average $\langle \ldots \rangle$ is over the distribution of θ values present in the sample, or a "powder average". Note that because of the axial symmetry of the fast motions, only the dependence

on angle θ remains, which is the angle between the axis of symmetry of the molecule (the normal to the bilayer) and the external magnetic field.

For phospholipid molecules containing many inequivalent C–D bond sites within each molecule, not a single S_{CD} value but rather a distribution of order parameters, $S_{CD}(n)$, where n is the index of the carbon position along the fatty-acid chain of the phospolipid, for example, is needed. Since the carbons at the end of the fatty acids chains away from the glycerol backbone are more free to move, the order parameters tend to decrease towards the terminal methyl group. On average, phospholipids with shorter fatty-acid chains are more ordered, *i.e.* exhibit a higher average values of S_{CD}. Thus, a distribution of quadrupolar splittings in a sample provides a direct measure of the distribution of order parameters, and therefore, of the range of motional environments available to various parts of the phospholipid molecule. This allows us to investigate both molecular alignment in the sample and its reorientational dynamics.

2.5 Distribution functions and powder spectra

Experimentally observed spectrum is a function of both θ, the angle between the local molecular axis and the external magnetic field, and the anisotropy parameter $x = \omega_q S_{CD}$. For each value of the anisotropy parameter (*e.g.*, for each C–D bond) the observed quadrupolar splitting is related to x through a $P_2(\cos)$ scaling of Eq. 2.19 [27, 38]. The observed powder spectrum contains contributions from many x and θ values, and so must be described by both an anisotropy distribution function, $g(x)$, and an orientational distribution function, $p(\theta)$:

$$S(\omega) = \int g(x)[p(\theta)\frac{\partial\theta}{\partial\omega}]\,dx\,, \quad x(\theta,\omega) \tag{2.20}$$

$$= \int p(\theta)[g(x)\frac{\partial x}{\partial\omega}]\,d\theta, \quad \theta(\omega,x) \tag{2.21}$$

Here, Eq. 2.21 is a $g(x)$-weighted superposition of lineshape functions, one for each anisotropy, x, while Eq. 2.21 is a $p(\theta)$-weighted superposition of spectra from the individual domains

that make up a powder sample, one from each of the orientations θ.

For a highly oriented sample, $p(\theta) = \delta(\theta)$. For an isotropic orientational distribution, $p(\theta) \propto \sin(\theta)$, and the lineshape function,

$$p(\theta)\frac{\partial\theta}{\partial\omega} = -\frac{p[\theta(x,\omega)]}{[2(x-\omega)(x+2\omega]^{1/2}} \quad , \tag{2.22}$$

can be obtained directly from Eq. 2.19, as illustrated in Fig. 2.4 for both spin-$\frac{1}{2}$ and spin-1. For historical reasons, lineshapes such as the one shown in Fig. 2.4b, are called "Pake doublets", or more generally, Pake patterns, after G.E.Pake [23].

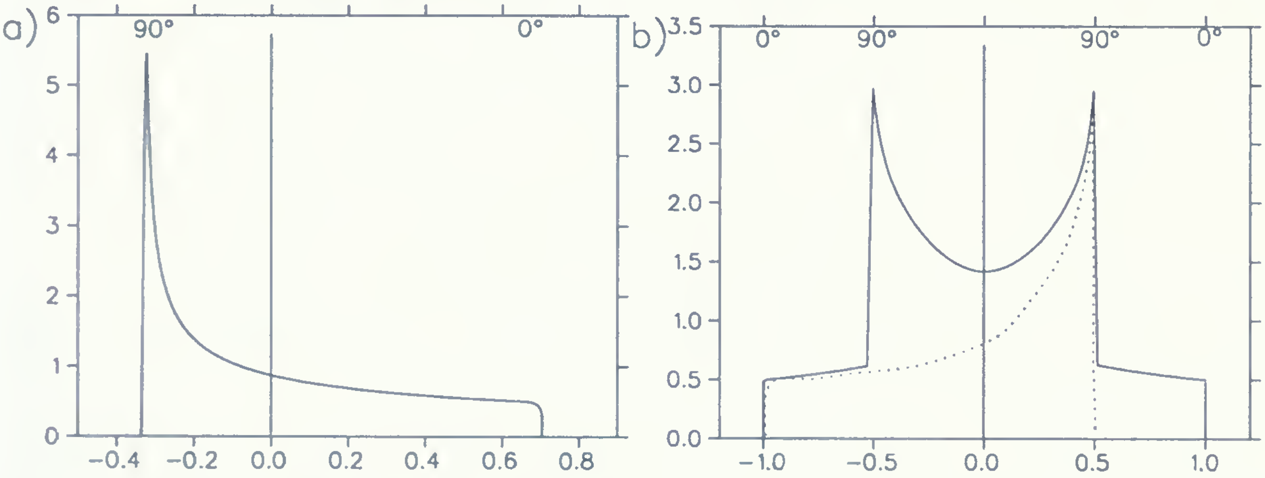

Figure 2.4: **Powder patterns.** (**a**) A general line shape for spin-$\frac{1}{2}$. (**b**) For spin-1, the spectral line shape can be thought of as a superposition of two spin-$\frac{1}{2}$ spectra, one for each of the two lines in a quadrupolar doublet. Note a characteristic "peak" in the intensity that corresponds to $\theta = 90°$. Reproduced from [13]

For a distribution of anisotropies, the NMR spectrum is a superposition of several such Pake patterns, one for each value of x present in the system. An experimental spectrum of d_{54}-DMPC (chain-deuterated DMPC) at 35°is shown in Fig.2.5 as an example; here the spectrum is a superposition of 54 different Pake patterns (some have equivalent x values and are not distinguishable).

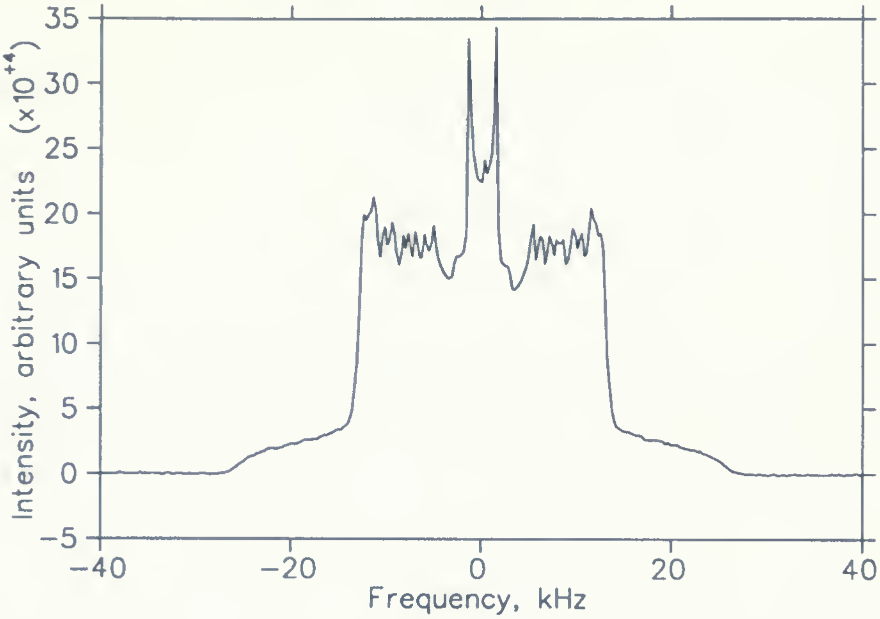

Figure 2.5: d_{54}-DMPC powder pattern at 35°C [13]

2.6 DePakeing via Tikhonov regularization

Obtaining the distribution of anisotropies $g(x)$ from the experimentally measured spectrum, $S(\omega)$, is essentially an inversion of Eqs.2.21–2.21, and is referred to as de-Pake-ing [3, 36]. Re-writing Eq. 2.21 as

$$S(\omega) = \int g(x) C(x,\omega)\, dx \quad , \tag{2.23}$$

where $C(x,\omega)$ is the kernel function:

$$C(x,\omega) = \begin{cases} p(\theta)\frac{\partial\theta}{\partial\omega}, & \text{for} - x/2 < \omega \leq x \\ 0, & \text{otherwise} \end{cases} \tag{2.24}$$

one can see that a solution of a Fredholm integral equation of the first kind is needed. This is a mathematically ill-posed problem. However, several numerical strategies exist for obtaining an approximate solution [29]. If $p(\theta)$ is known, then a traditional iterative algorithm can be used [36]. If $g(x)$ is known, the problem can be solved for an unknown $p(\theta)$, as in the case of the orientational distribution function of a nematic liquid crystal trapped in the channels of microporous material [28]. Even when both $g(x)$ and $p(\theta)$ are not known, Tikhonov

regularization can be used to obtain both distribution functions simultaneously [38].

An essential summary of the Tikhonov regularization algorithm is as follows. Assuming that the experimental discretely sampled data are made up of the "true" data S_j and a random noise σ_j,

$$S_j{}^\sigma = S_j + \sigma_j \tag{2.25}$$

the best fit is obtained through the minimization of the following expanded least-squares expression, with respect to $g(x)$:

$$\Psi[g(x)] = \sum_{j=1}^{m}[S_j^\sigma - S_j]^2 + \lambda||g||^2 \quad . \tag{2.26}$$

Here the first term is the least-squares misfit that assures compatibility with the experimental data. The second term controls the smoothness of the fit, with λ being the regularization parameter. The quality of the approximate solution $\tilde{g}(x)$ depends on choosing an appropriate value for this parameter. Too big a λ suppresses the information in the solution and too small a λ gives us a physically meaningless answer. To determine an appropriate λ, self-consistency method is used which is estimating λ from the experimentally noisy data [16]. By using the estimated λ, $\tilde{g}(x)$ will be obtained from minimizing $\Psi[g(x)]$.

Different models for $p(\theta)$

For a simultaneous determination of both $g(x)$ and $p(\theta)$ an appropriate parameterization of $p(\theta)$ must be used, containing a limited number of parameters. In the simplest case, just one parameter, κ, is used. If κ is chosen appropriately, $p_\kappa(\theta)$ approximates the true orientational distribution function. $p_\kappa(\theta)$ is well-defined for each κ so by using the experimental data, $S_j{}^\sigma$, $\tilde{g}(x)$ can be determined by using Tikhonov regularization method; so equation 2.26 changes to

$$\Psi(\kappa) = \Psi[g(x); \kappa] = \int [S(\omega)^\sigma - S(\omega)_{(\tilde{g}(x),\tilde{\kappa})}]^2 + \lambda||g||^2 \tag{2.27}$$

subject to $g(x) \geq 0$. Stepping through a range of values for κ allows finding the optimum estimate of κ. Using this κ, $p_{\tilde{\kappa}}(\theta)$ which is close to the true $p(\theta)$ would be determined and

then the best approximation for $\tilde{g}_{\tilde{\kappa}}(x)$ within the limits defined by $p_\kappa(\theta)$ model. Different models are used to get the lowest minimum of the misfit among all different model functions. Some possible one-parameter models are [38]:

ellipsoidal model can be visualized as a continuous deformation of spherical model. Here κ_E is the square of the ratio of the semi-axes of the ellipsoid. Obviously $\kappa_E = 1$ describes a sphere; $\kappa_E > 1$ describes an ellipsoid with the long axis parallel to the external magnetic field. The orientational distribution function is:

$$p_E(\theta) \propto \sin\theta \times [1 - (1 - \kappa_E)\cos^2\theta]^{-2} \tag{2.28}$$

Legendre model is a truncation of the Legendre polynomial expansion:

$$p_L(\theta) \propto \sin\theta \times (1 + \kappa_L \cos^2\theta) \tag{2.29}$$

$\kappa_L = 0$ corresponds to the random (spherical) distribution spherical.

Boltzmann model assumes that the probability of encountering a domain at a particular orientation is given by the Boltzmann factor associated with the energy of interaction between this domain and the external magnetic field. In this model the adjacent domains have totally uncorrelated orientations. Again, $\kappa_B = 0$ corresponds to a random distribution and $|\kappa_B| \gg 1$ shows a perfect alignment.

$$p_B(\theta) \propto \sin\theta \times exp(\kappa_B \cos^2\theta) \tag{2.30}$$

If we assume that $\kappa_L = \kappa_B = 2(1 - \kappa_E)$ and we expand the $\cos^2\theta$ in equation 2.28 and 2.30, then for a small deviation from random distribution all three models yield the same result, as expected. For any given spectrum, all three models can be tested; the global minimum of the misfit function with respect to the choice of the model, and of the parameter characterizing the model, corresponds to the best fit and thus to the best model to describe alignment of the molecular domains in the sample.

Chapter 3

Synthesis of deuterated chlorhexidine

Chlorhexidine was first marketed as the active ingredient of an antiseptic cream for use on skin wounds in 1954. Other preparations containing chlorhexdine have been used as typical disinfectants since mid-1970s. As an anti-bacterial agent it is used in mouth rinses and in dental care.

Chlorhexidine was first synthesized by Rose and Swain in 1956, using two different synthetic pathways. One required a reaction of nitrobenzene with N–phenylcyanoguanidine at each of the amino groups of a diamine; the second was the complementary process in which *bis*–cyanoguanidine interacts with two molecular proportions of the amine NHRR′[26]. Synthesis of ^{14}C-labeled chlorhexidine was reported by Burns [5] using a different synthetic pathway, illustrated in Fig.3.1. However none of the three pathways could be used directly for the synthesis of the ^{2}H-labeled analogue: deuterated N–phenylcyanoguanidine [26] or 1,4-di-iodobutane [5] are not readily available. In addition, the Burn's pathway begins with a fully saturated protonated material, and deuterium substitution in saturated compounds is problematic. Finally, each of the three pathways involves multiple solvents and intermediate reagents that would also have to be replaced by their deuterated analogs, to prevent exchange with their protons. Thus an alternative synthetic pathway is required.

Several ways of synthesizing deuterated chlorhexidine were considered, in consultation with Prof. T.Hudlicky and Dr. M.Moser (Department of Chemistry, Brock University) and finally the appropriate way was performed by Dr. M.Moser and S.Sadeghi. One possibility, illustrated in Fig.3.2, unfortunately failed when the amine could not be brought out from the alcohol (steps 4 → 6). Another pathway, shown partially in Fig.3.3, was followed up to

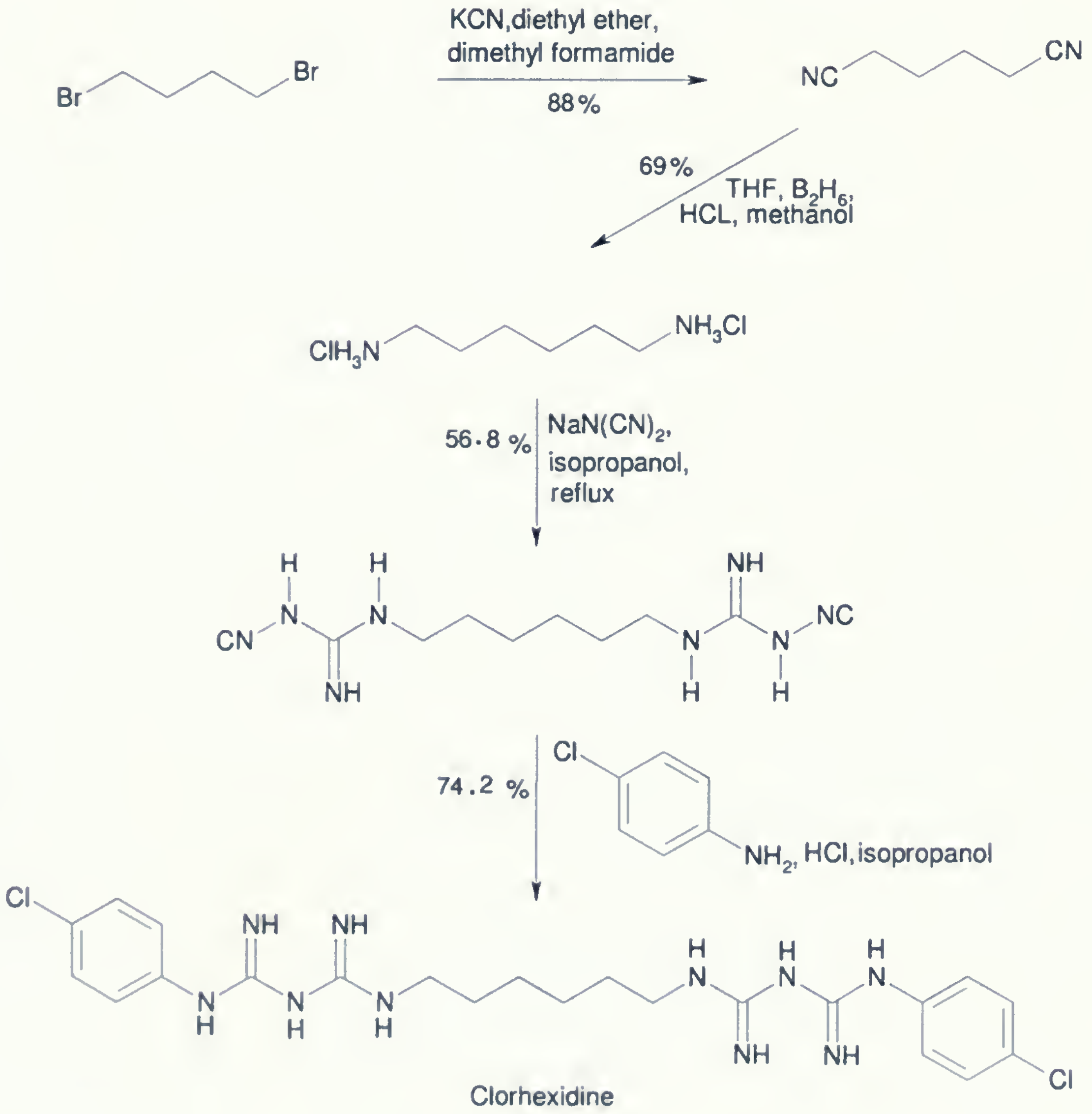
Br
Br
KCN,diethyl ether,
dimethyl formamide
88%
NC
CN
69%
THF, B2H6,
HCL, methanol
ClH3N
NH3Cl
56.8 %
NaN(CN)2,
isopropanol,
reflux
CN
NC
74.2 %
Cl
NH2, HCl,isopropanol
Clorhexidine

Figure 3.1: Synthesis of ^{14}C-labeled chlorhexidine as reported by Burns [5].

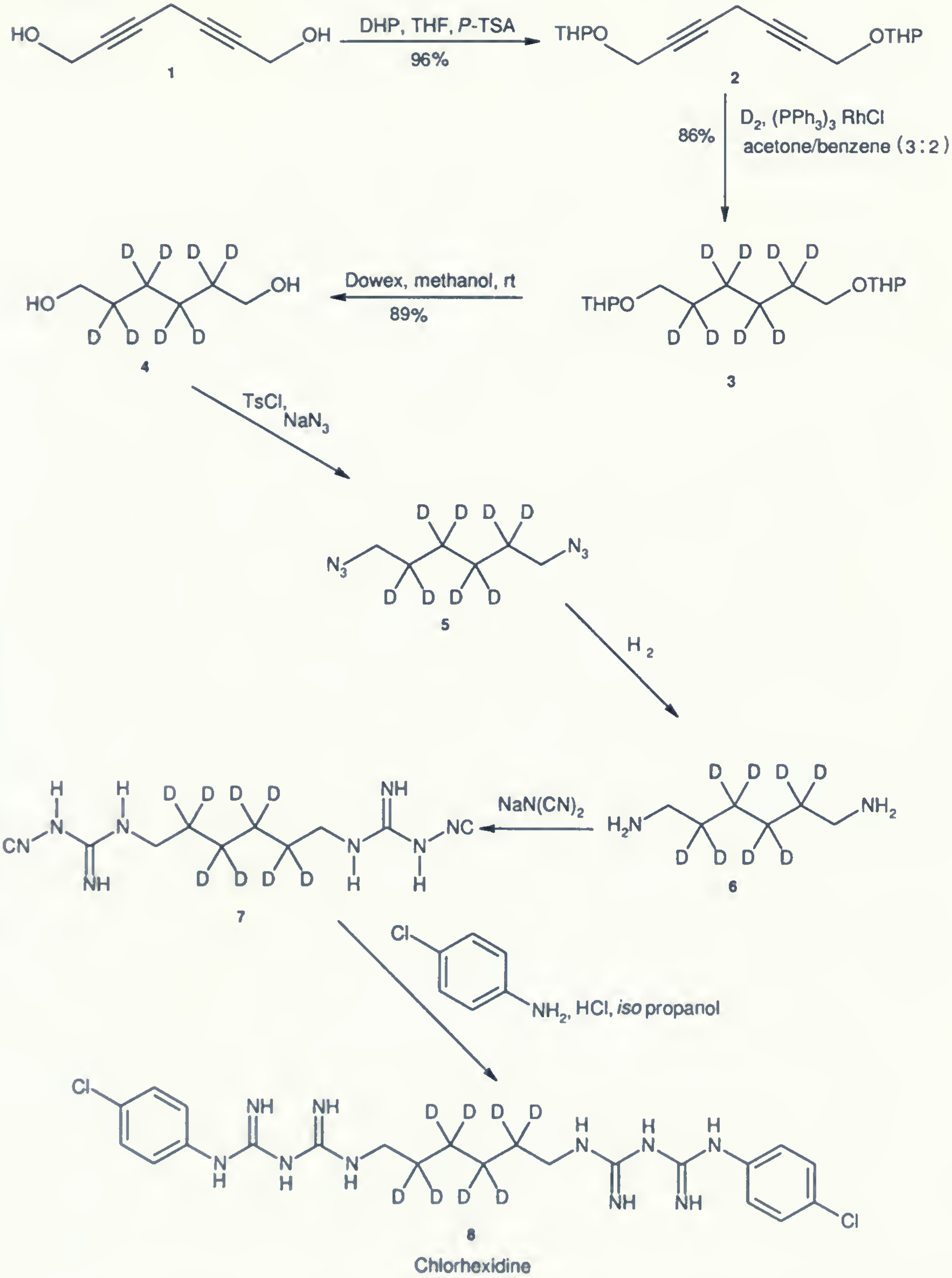
HO
OH
1
DHP, THF, P-TSA
96%
THPO
OTHP
2
86%
D2, (PPh3)3 RhCl
acetone/benzene (3:2)
3
Dowex, methanol, rt
89%
4
TsCl, NaN3
N3
5
H2
H2N
NH2
6
NaN(CN)2
CN
NC
NH
7
Cl
NH2, HCl, isopropanol
8
Chlorhexidine

Figure 3.2: First attempted synthesis of deuterated chlorhexidine.

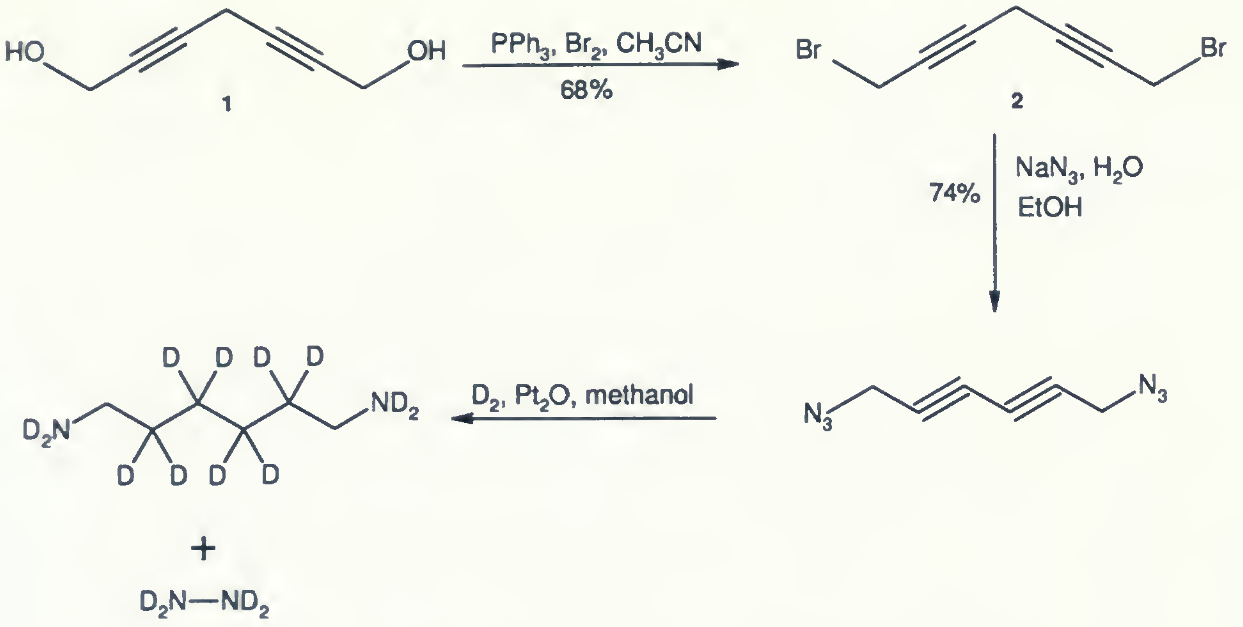

Figure 3.3: Second attempted synthesis of deuterated chlorhexidine.

the step of obtaining 6-hexanediamine dihydrochloride, where deuterium atoms were lost to exchange with non-deuterated methanol. Potentially, this remains a promising pathway, but we had no deuterated methanol available to pursue it further.

Instead, the process illustrated in Fig.3.4 was used to obtain deuterated chlorhexidine. The initial reagents: tris(triphenylphosphine)-rhodium(I)chloride, sodium azide, sodium dicyanamide and sodium chloraniline were purchased from Sigma-Aldrich (Oakville, ON); the deuterium gas was provided by Praxair (Hamilton, ON). In the following step-by-step description of the process, the numbers correspond to those used in Fig.3.4:

1. **2,4-Hexadiyne-1,6-diol** was purchased from ScienceLab.com (Houston, Texas).

2. **Bis-1,6-(tetrahydropyran-2-yloxy)-2,4-hexadiyne**. A solution 10% (W—V) of *p*-toluenesulphonic acid in tetrahydrofuran was added to a mixture of (1), dry tetrahydrofuran, and freshly-distilled 2,3-hydropyran, and then stirred for one hour at 0°C. Followed by a further 24 hours at room temperature. Anhydrous potassium carbonate was added and the mixture stirred for a further seven hours at room temperature. A yellow oily residue was obtained after filtering off the salts, and evaporating to dryness.

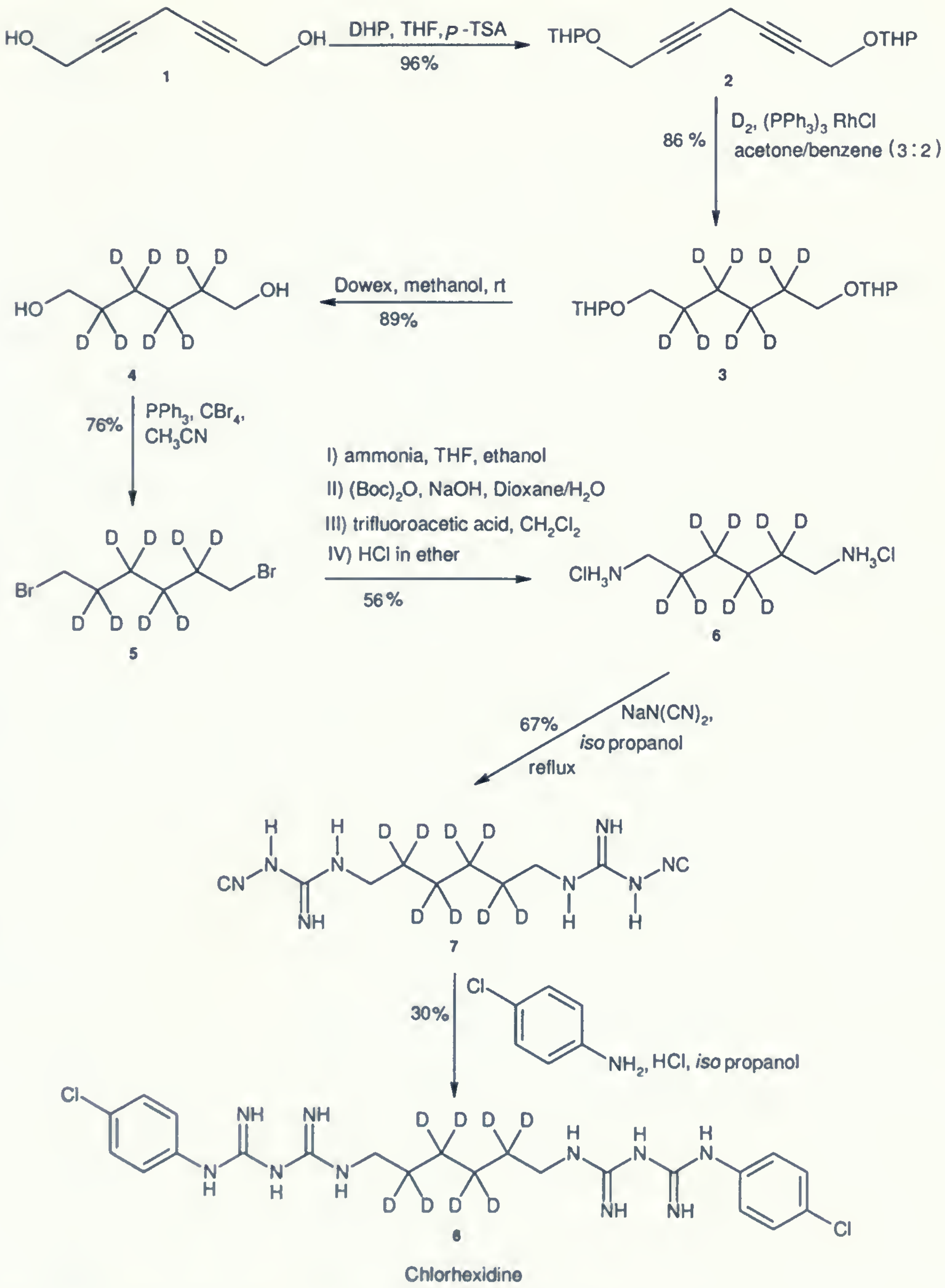
HO
OH
1
DHP, THF, p-TSA
96%
THPO
OTHP
2
86 %
D2, (PPh3)3 RhCl
acetone/benzene (3 : 2)
D D D D
THPO
OTHP
D D D D
3
Dowex, methanol, rt
89%
D D D D
HO
OH
D D D D
4
76%
PPh3, CBr4,
CH3CN
D D D D
Br
Br
D D D D
5
I) ammonia, THF, ethanol
II) (Boc)2O, NaOH, Dioxane/H2O
III) trifluoroacetic acid, CH2Cl2
IV) HCl in ether
56%
D D D D
ClH3N
NH3Cl
D D D D
6
67%
NaN(CN)2,
iso propanol
reflux
H
H
D D D D
NH
CN
N
N
N
N
NC
NH
D D D D
H
H
7
30%
Cl
NH2, HCl, iso propanol
Cl
NH
NH
D D D D
H
H
H
N
N
N
N
N
N
H
H
H
D D D D
NH
NH
Cl
8
Chlorhexidine

Figure 3.4: The chemical pathway used for the synthesis of deuterated chlorhexidine.

The yellow residue was added to the mobile phase EtOAc/n-hexane (2:3) and filtered through a column of 12.5 g alumina and 6.25 g of SiO_2. The alumina was in the lower, and SiO_2 — in the upper layer. The same solvent system was used for the purification by column chromatography over silica. The solvents were evaporated and the residue was dried in vacuo for one hour [11].Yield was 96%.

3. **2,2,3,3,4,4,5,5,5-($^2H_8$)-Bis-1,6-(tetrahydropyran-2-yloxy)-hexane**. To vigorously stirred deuterium purged solution of tris(triphenylphosphine)-rhodium(I)chloride(1.28 g), in 75 ml of acetone/benzene (3:2) was added 5.05 g (18.1 mmol) of (2) in a solution of 50 ml of the same solvent mixture, at room temperature under a deuterium atmosphere. After 20 hours the solvents were removed via distillation, 25 ml of *n*-hexane was added and the resulting suspension was filtered through alumina (TSC Wolem, *ca.* 50 g), and eluted with *n*-hexane. The solvent was removed in vacuo (1 hour, 50°C, 0.1 mm) to obtain pure (3) as a colourless oil [11]. Yield was 86%.

4. **2,2,3,3,4,4,5,5-($^2H_8$)-Hexane-1,6-diol**. A mixture of (3) (4.60 g), methanol (81 ml) and cation exchange resin (Dowex AG 50W-X8, 1.35 g) was stirred for 12 hours at room temperature. Filtration, evaporation and drying (1 hour, 0.1 mm) gave an oil which gradually solidified in the refrigerator. Recrystallization from EtOAc/n-hexane provided colourless crystals [11].Yield was 89%.

5. **2,2,3,3,4,4,5,5-($^2H_8$)-Hexane-1,6-dibromide**. To a suspension of triphenylphosphine (4.90g; 18.7 mmol) in 18.5 ml anhydrous acetonitrile cooled in an ice bath, bromine (2.92 g;18.2 mmol) was added drop-wise with stirring at such a rate that the mixture remains colourless. After the addition was complete the supernatant solution was slightly yellow. The ice bath was removed and a solution of alkynediol (4) (1.15 g;9.1 mmol) in 10 ml acetonitrile was added with stirring over a period of 15 min. The temperature of the mixture rose to 40–50°C and the precipitate dissolved completely for a short time. After the mixture cooled down to room temperature again the

bulk of the solvent was stripped off in a rotary evaporator, and the residue was suspended in dry ether, filtered, and the collected solids were carefully washed five times with small portions of ether. The ether solution was concentrated and the residue distilled under reduced pressure (Kugelrohr at 130°C, 0.1 torr) [25]. Yield of this step was 1.75 g (6.9 mmol, 76%).

^{1}H-NMR: ($CDCl_3$) 3.97 (s,4H). ^{13}C-NMR: ($CDCl_3$) 33.5; There was no signal for C of C–D bonds.

6. **2,2,3,3,4,4,5,5-($^2H_8$)-Hexane-1,6-diamine dihydrochloride.** To a solution of 800 mg dibromide from the previous step (3.2 mmol) in 110 ml THF/ethanol (1:1), 55 ml concentrated ammonia was added and the reaction mixture was stirred for 48 hours. The solvent was removed under reduced pressure and the resulting solid was suspended in a solution of 0.55 g NaOH in 55 ml dioxane/H_2O (1:1). The suspension was treated with Boc_2O (3.01 g; 13.8 mmol) at 0°C for one hour and then stirred at room temperature for further three hours. The reaction mixture was extracted with CH_2Cl_2 (3 × 40 ml) and the solvent was removed under reduced pressure. The resulting mixture was purified by column chromatography (hexane:ethyl acetate 7:3 + 0.1 % NEt_3). The obtained product was dissolved in 20 ml CH_2Cl_2, 5 ml trifluoroacetic acid were added and the solution was stirred over night. After evaporation to dryness 50 ml saturated HCl ether solution was added. The solution was evaporated to dryness and the cycle was repeated for further two times. The product was obtained as white crystals. Yield of this step was 350 mg (1.8 mmol, 56%) [30].

   ^{1}H-NMR: ($CDCl_3$) 7.90 (br s,6H); 2.74 (s,4H) MS:(Gly matrix) 125(M^+-2HCl).

7. **6-Hexamethylene bis (dicyandiamide),(HMBDA).** Diamine dihydrochloride, sodium dicyanamide (96%), and isopropanol pre-dried over molecular sieve (7 ml) were stirred and reflux for 16 hours (bath temperature (90–100°C), and then heated for 20 hours at 85°C. The white suspension was centrifuged to separate, and the product washed

with water (3 × 5 ml) before drying under reduced pressure at 45°C for 16 hours, to give a white solid [5]. Yield: 67%.

8. **Deuterated chlorhexidine**. p-Chloroaniline (263 mg, 2.075 mmol) was stirred with *iso*propanol (1 ml). A solution of concentrated hydrochloric acid in *iso*propanol (192 mg in 1 ml) was added, and the mixture stirred for 30 minutes to give a clear solution. 268 mg of (7) and *iso*propanol were introduced into the reaction mixture which was then stirred in a silicone bath for seven hours at 85–90°C. After cooling the white gelatinous product was stirred at ambient temperature for 12 hours. On addition of an aqueous sodium hydroxide solution (2.7%, 3.3 ml) the white dihydrochloride dissolved and the crude chlorhexidine base was slowly deposited during two hours. The product was separated by centrifugation and washed with *iso*propanol (2 × 0.7 ml), *iso*propanol-water (1:1) (2 × 0.7 ml) and water (4 × 0.7 ml) before being dried under reduced pressure at ambient temperature for 16 hours. This gave a solid, 238 mg. The white solid was recrystallized from ethanol (freshly distilled) eight times. Yield: 30%.

   TLC shows a single spot in toluene:ammonia:methanol 60:20:70 [5]. ^{1}H NMR confirms that the final product is chlorhexidine (see Fig.3.5); a small amount of residual H_2O is also seen. Yield: 162 mg (0.316 mmol).

   ^{1}H-NMR: (DMSO); 9.87(1H,br s,NH); 9.54(1H,br s,NH); 8.04(1H,br s,NH); 7.70(3H,br m,NH); 7.25,7.10(2H,br s,NH); 6.77(2H,br s,NH); 7.34(8H,m,CH); 3.07(4H,d,CH_2).

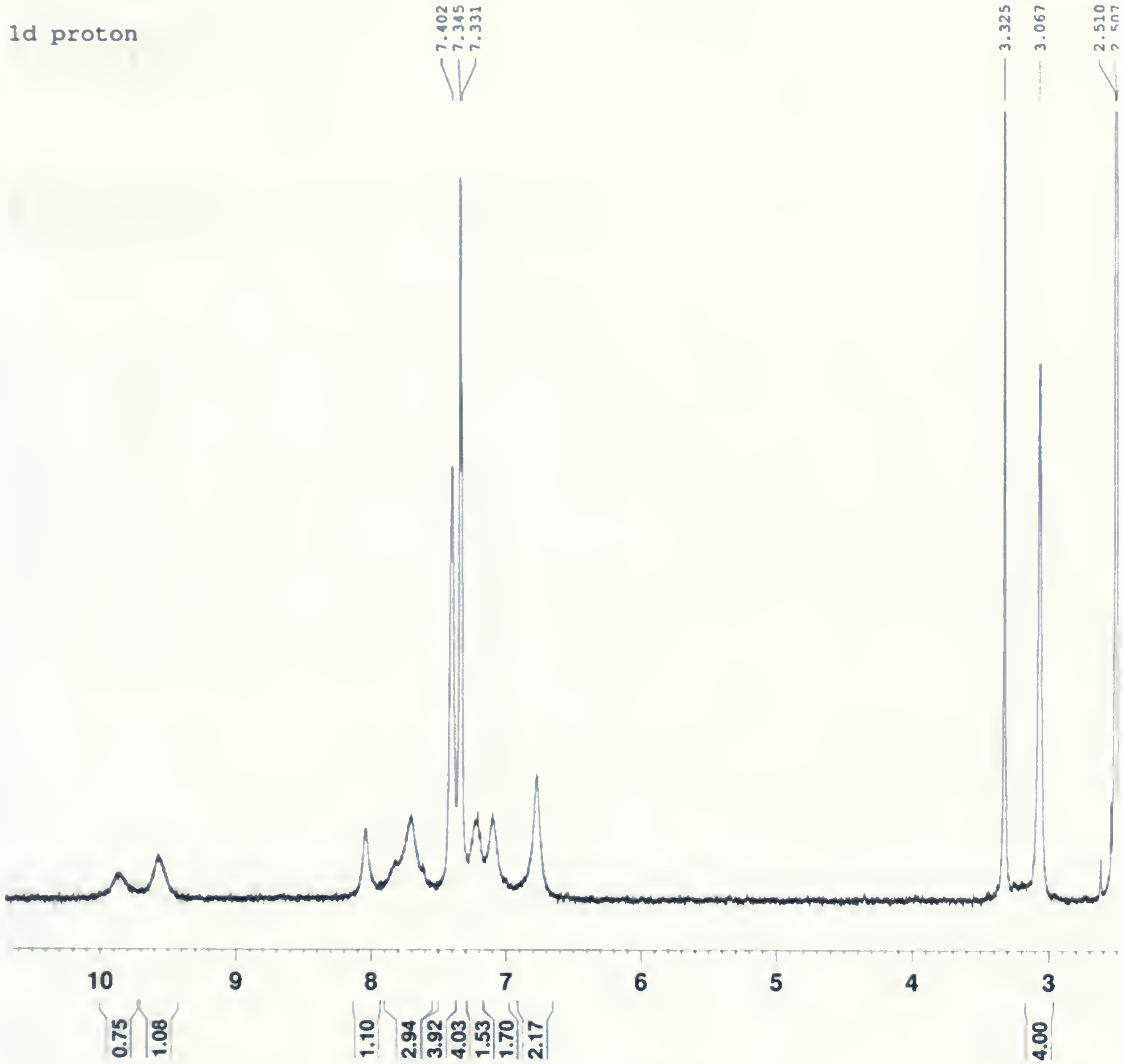

Figure 3.5: **^{1}H NMR spectrum of chlorhexidine deuterated in the saturated-chain methylenes.** The peak at 2.51 ppm is the reference solvent, DMSO. A small amount of H_2O is seen at 3.325 ppm. Small peaks at 1.2–1.5 ppm are from protonated methylene groups, and thus allow us to estimate the level of deuteration in the final product; from the ratio of the integral peak intensity to that of the protonated methylene adjacent to amine (at 3.067 ppm) we estimate the deuteration of about 95%. Since the two peaks at 1.2–1.5 ppm appear approximately equal in magnitude, the residual protons are randomly distributed among the various chain methylene sites.

Chapter 4

Experimental results

Lipid-chlorhexidine mixtures used in this study were prepared using the deuterated d_{54}-1,2-dimyristoyl-glycero-3-phosphocholine (d_{54}-DMPC) purchased from Avanti Polar Lipids (Alabaster, AL, USA) and used without further purification. The chain-deuterated analog has all hydrogen atoms on the 13 lower carbon positions of both of its fatty acid chains replaced with deuterium atoms. This lipid is well-known in the field of model membranes [10]. The molecular structure is shown in Fig.4.1.

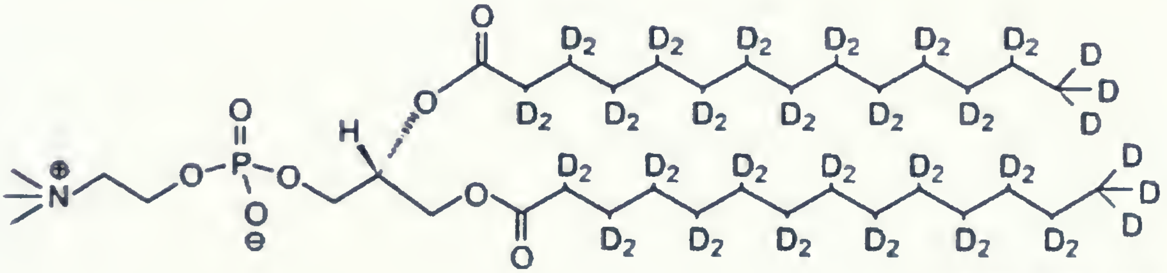

©Avanti Polar Lipids

Figure 4.1: 1,2-dimyristoyl-d_{54}-glycero-3-phosphocholine (DMPC-d_{54}) Reproduced from `www.Avantilipids.com`

Chlorhexidine, as chlorhexidine digluconate (CHG), was purchased from Sigma Aldrich (Oakville, ON, Canada) and used without further purification. In this form, chlorhexidine is soluble in water allowing for a preparation of stock solution to simplify the sample preparation. Deuterium-depleted water was purchased from Cambridge Isotope Laboratories Inc. (Andover, MA, USA).

All samples were prepared following the same protocol. Powder of d_{54}-DMPC was dried

for several hours at reduced pressure (10^{-4} torr) immediately prior to use. Each sample typically contained 35 mg of lipid which was mixed with an appropriate amount of a 20% solution of chlorhexidine digluconate (CHG) under the Nitrogen atmosphere ($[O_2] < 0.2\%$). Additional water was then added to bring the total (lipid+chlorhexidine):water ratio to 30:70 by weight,

$$\frac{m_{H_2O}}{m_{CHG} + m_{DMPC-d_{54}}} \quad .$$

The samples were prepared in snap-closure polyethylene containers which were then sealed with a soldering iron. This proved inadequate in some cases, especially for samples that were brought up to high temperatures, and an occasional leakage and loss of water was observed. The weight of the sample was recorded before and after each set of experiments and if a loss of weight was observed, the results were not used.

Samples of two different lipid:chlorhexidine molar ratios were used, $x = 3 : 1$, and $x = 10 : 1$, where

$$x = \frac{[DMPC - d_{54}]_{mol}}{[CHG]_{mol}} \quad .$$

Following preparation, the mixing of the sealed samples was achieved by several (at least five) cycles of freezing the sample in a dry-ice/ethanol or a liquid nitrogen bath, followed by a thawing in a warm water bath. As the sample melted, it was gently vortexed. All samples achieved uniform semi-translucent appearance at the end of this procedure. Following preparation the samples were equilibrated at 4°C for several days.

4.1 NMR spectroscopy

NMR measurements were performed using a home-built spectrometer with a 7.0-T Oxford Instruments superconducting magnet, using an inductively-coupled probe. Details of the spectrometer design can be found in [34].

The temperature in the probe was set and maintained by an airflow temperature controller, based on Omega CN76000. The temperature was maintained constant throughout

each experiment to within ±0.2°C. After changing the temperature to a new setting, data acquisition was always performed following an equilibration for at least 45 mins at the target temperature in the spectrometer. The spectra were monitored and some extremely long equilibration times were seen. At some temperatures the $x = 3 : 1$ samples required up to two hours of equilibration before a reproducible spectrum could be measured.

The ^{2}H NMR experiments were performed at a frequency of 46.06 MHz.

Quadrupolar echo sequence [8] was used to avoid an unusually long dead time of the receiver that we observed in these samples in our spectrometer. We found that the minimum inter-pulse delay that would yield a clean spectrum free of magneto-acoustic ringing was $\tau = 130\ \mu$s. A series of quadrupolar-echo experiments with varying τ was measured with a small number of scans for each, and the time-domain peak echo intensities recorded and fitted to an exponential decay curve, yielding a measurement of T_2^{qe}. These were collected in a pseudo-random order in τ values, typically 300, 140, 800, 500, 180, 200, 150, 600, 250, and 400 μs. The spectra were obtained by using $\tau = 180\ \mu$s and 6000 scans each, using an 8-C "CYCLOPS" phase cycling scheme [24] and processed using the DANS software [35]. Typical repetition time was 800 ms and the dwell time of 5 μs. The length of the 90° pulse was 2.0–2.1 μs.

Inversion recovery technique modified as appropriate for the quadrupolar ^{2}H NMR [33] was used to measure T_{1z}. The quadrupolar-echo delay τ_2 was kept at 180μs and τ_1 values were varied in a pseudo-random order: 10, 4, 8, 250, 100, 40 ms. At some temperatures, two-exponential four-parameter fits were necessary to fit the decay curves; one-exponential two-parameter (amplitude and decay time constant) fits were used in all other cases. All fitting and preparation of the figures for this thesis was made using the `physica` software (TRIUMF, Vancouver, BC).

4.2 Spectral moments

The method of moments was used to monitor temperature-induced changes in NMR spectra. Generally unnormalized moments are defined as:

$$M_n(\omega) = \frac{\int (\omega - \omega_0)^n S(\omega) d\omega}{\int S(\omega) d\omega} \tag{4.1}$$

where $S(\omega)$ is the spectrum. Clearly, for a symmetric spectrum all odd moments vanish. The second moment is a good measure of the average spectral width. Monitoring the second moment as a function of temperature is a good indicator of the thermodynamic changes occurring in the sample.

4.3 ^{2}H NMR spectra

Representative spectra for the $x = 3:1$ and $x = 10:1$ samples are shown in Fig.4.2 and Fig.4.3, respectively. Note that for both samples the first heating cycle spectra are different from the subsequent heating and cooling cycles. This is especially clear when comparing the temperature dependence of the second moments through the various heating/cooling runs, as shown in Fig.4.4. It is a general feature of these samples that after the first heating cycle the thermal hysteresis is reduced and the spectra are reproducible, with their second moments within an error bar of each other. Despite several attempts, this feature could not be eliminated by prolonged pre-equilibration at a single elevated temperature; its seems that a slow step-wise heating cycle is required to fully equilibrate the system. The error bars in Fig.4.4 were calculated by changing the limits of the numerical integration (typically, about 700 points) by ±50 points.

4.4 T_{1z} and relaxation

Complicated thermal behaviour of our lipid:chlorhexidine mixtures is confirmed by the relaxation measurements. Table 4.1 again illustrates the importance of a slow first heating

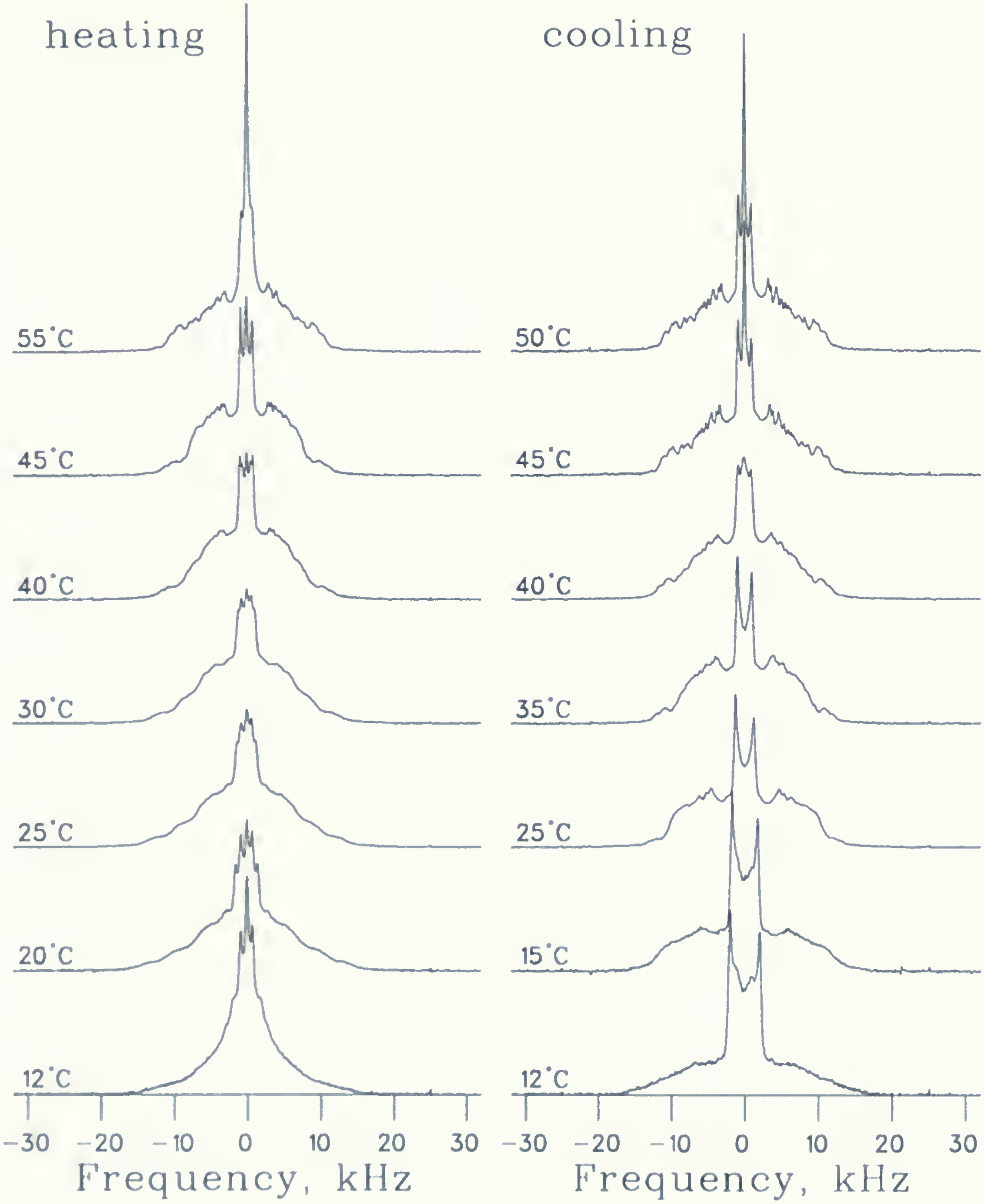

Figure 4.2: Representative ^{2}H NMR spectra for the $x = 3:1$ samples

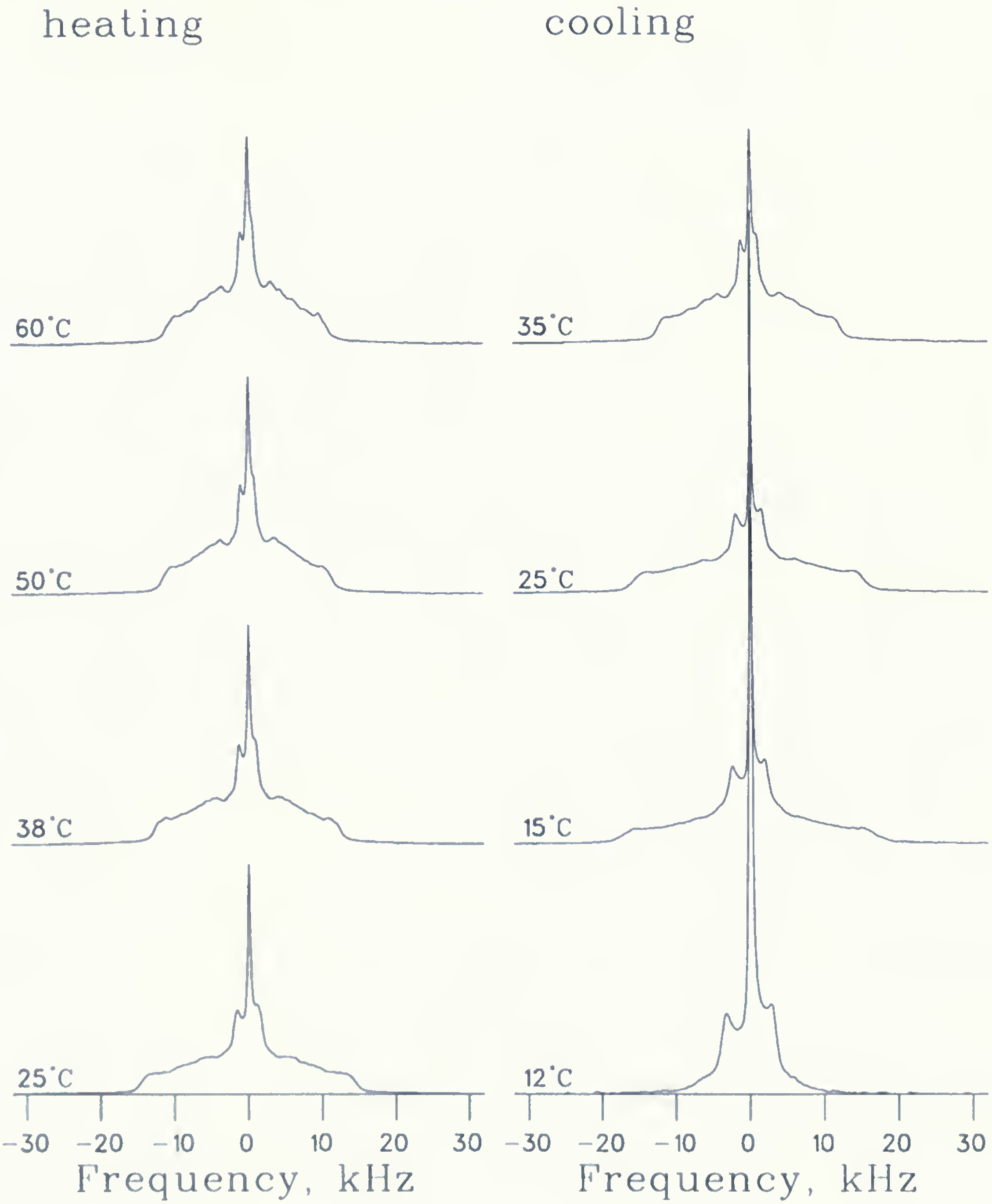

Figure 4.3: Representative ^{2}H NMR spectra for the $x = 10:1$ samples

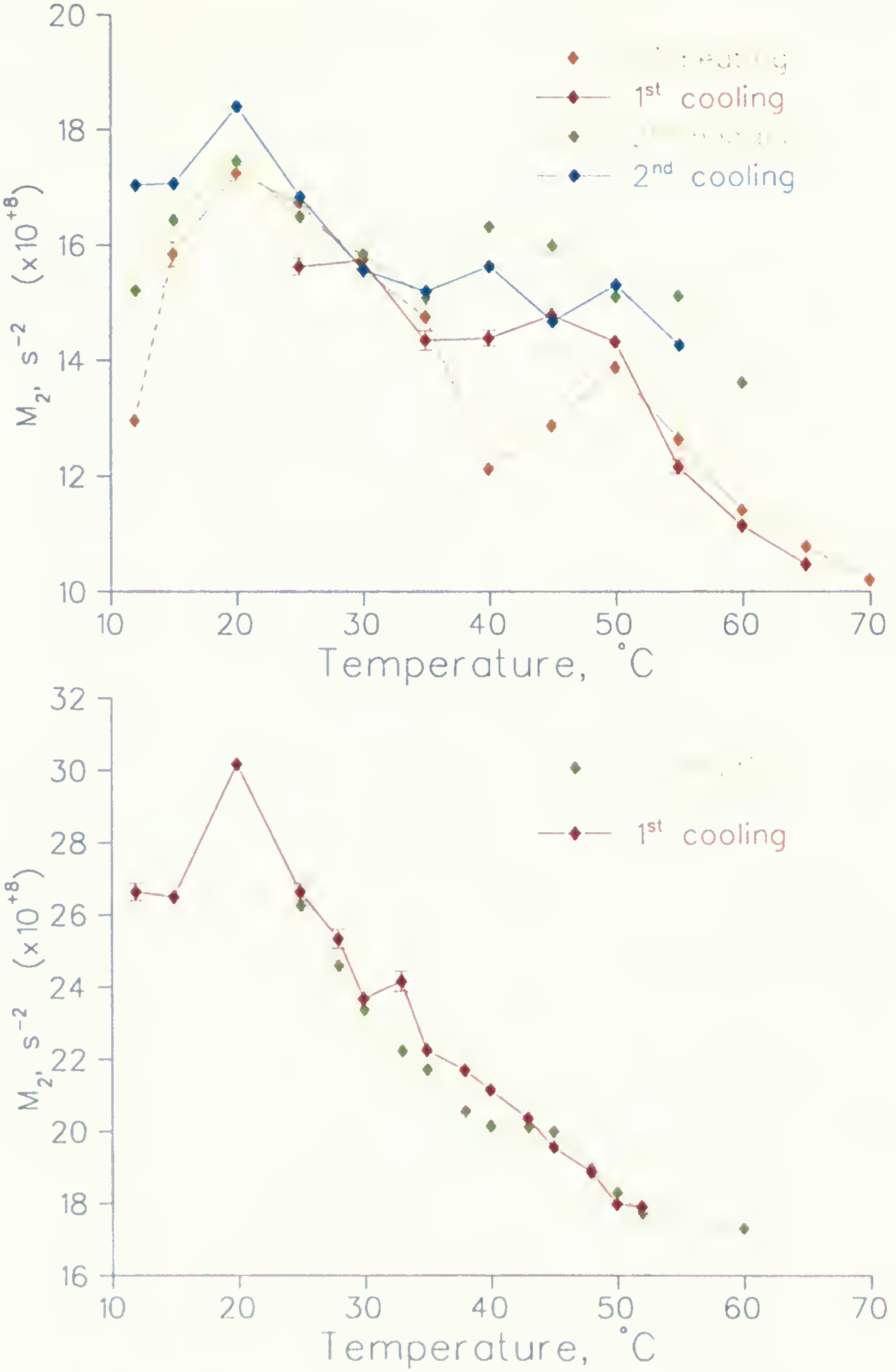

Figure 4.4: The temperature dependence of the second moments of the spectra for the $x = 3:1$ (top) and $x = 10:1$ (bottom) samples through the various heating/cooling runs

Table 4.1: **Thermal history of T_2^{qe} of the 3:1 sample.** Evidence of thermal hysteresis, as indicated by an exponential fit to the quadrupolar echo decay data. Note that the first heating produces different T_2 values from those of the first cooling and subsequent heating and cooling cycles, which are all within an error bar of each other. $\tau_{90} = 2.0\,\mu$s, repeat time 800 ms.

$t \pm 0.2$, °C	T_2^{qe}, ms (first cycle)	T_2^{qe}, ms (second cycle)
12.0	0.534 ± 0.012	0.585 ± 0.010
15.0	0.572 ± 0.008	0.614 ± 0.014
20.0	0.647 ± 0.010	0.655 ± 0.008
25.0	0.704 ± 0.016	0.838 ± 0.009
30.0	0.763 ± 0.024	0.984 ± 0.018
35.0	0.774 ± 0.033	1.194 ± 0.019
40.0	0.826 ± 0.029	1.443 ± 0.016
45.0	0.970 ± 0.037	1.511 ± 0.030
50.0	1.114 ± 0.024	1.460 ± 0.025
55.0	1.122 ± 0.025	1.383 ± 0.025
60.0	1.140 ± 0.029	1.320 ± 0.031
65.0	1.122 ± 0.016	—
70.0	1.102 ± 0.018	—
65.0	1.082 ± 0.017	—
60.0	1.104 ± 0.015	—
55.0	1.176 ± 0.015	1.341 ± 0.035
50.0	1.286 ± 0.015	1.385 ± 0.025
45.0	1.362 ± 0.018	1.401 ± 0.016
40.0	1.275 ± 0.041	1.326 ± 0.014
35.0	1.149 ± 0.018	1.156 ± 0.013
30.0	1.106 ± 0.017	1.072 ± 0.015
25.0	0.899 ± 0.011	0.911 ± 0.021
20.0	—	0.747 ± 0.019
15.0	—	0.651 ± 0.019
12.0	—	0.557 ± 0.012

cycle before the equilibrium is reached. First cooling, and subsequent heating/cooling cycles are again reporting the T_2^{qe} values that are consistently within an error bar of each other; the initial heating cycle produces values that are significantly different. To avoid such thermal hysteresis, the measurements obtained during the first heating are not used in subsequent analysis. Table 4.2 contains the T_2^{qe} relaxation data for the $x = 10 : 1$ sample. Fig. 4.5 compares the results of the T_2 measurements for the $x = 3 : 1$ and $x = 10 : 1$ samples from Tables 4.1 and 4.2.

T_{1z} decay data most of the time required a two-exponential fit. It was hoped that this could be used to monitor possible coexistence of multiple structural phases in the samples. However, spectra did not show clear evidence of phase coexistence; The most likely origin of the two contributions to the T_{1z} is from the significantly longer T_{1z} associated with the terminal methyl groups of the DMPC. We did not acquire a sufficiently resolved set of points on the exponential decay curves to perform a refined multi-exponential analysis. The quality of the exponential fits that was available with the data that we had resulted in large error bars for T_{1z} values obtained through the exponential fits, as illustrated by a typical fit shown in Fig. 4.6, and it can only be used for illustrative purposes. A summary of the T_{1z} values obtained in this manner is presented in Tables 4.3 and 4.4.

4.5 De-Pake-ing and order parameter profiles

De-Pake-ing was performed using the `peakcern` de-Pake-ing package written by H.Schäfer and E.Sternin [38] using ellipsoidal model for a distribution of orientations, $p(\theta)$. Other models were tested and yielded similar results; for simplicity only the ellipsoidal model was used from then on. A typical result of de-Pake-ing is shown in Fig 4.7, where the red line is the measured spectrum and the green one is a powder pattern recalculated from the dePaked $g(x)$, for the spectrum of d_{54}-DMPC:Ch (10:1) at 35°C. The two lines are indistinguishable on the plot, demonstrating an excellent quality of the fit. The cyan line is the distribution

Table 4.2: **Thermal history of T_2^{qe} of 10:1 sample.** Evidence of thermal hysteresis, as indicated by an exponential fit to the quadrupolar echo decay data. T_2^{qe}s for the subsequent cycles are within the error bars of those of first cooling $\tau_{90} = 2.1$ μs, repeat time 800 ms.

$t \pm 0.2$, °C	T_2^{qe}, ms (first cycle)
25.0	0.821 ± 0.008
28.0	0.885 ± 0.015
30.0	0.928 ± 0.016
33.0	0.938 ± 0.014
35.0	0.931 ± 0.012
38.0	0.934 ± 0.012
40.0	0.908 ± 0.015
43.0	0.913 ± 0.009
45.0	0.896 ± 0.015
48.0	0.883 ± 0.014
50.0	0.882 ± 0.009
52.0	0.871 ± 0.009
55.0	0.879 ± 0.009
60.0	0.785 ± 0.008
55.0	—
52.0	0.886 ± 0.014
50.0	0.868 ± 0.015
48.0	0.892 ± 0.010
45.0	0.874 ± 0.016
43.0	0.883 ± 0.008
40.0	0.895 ± 0.017
38.0	0.893 ± 0.016
35.0	0.923 ± 0.011
33.0	0.931 ± 0.022
30.0	0.932 ± 0.012
28.0	0.953 ± 0.013
25.0	0.933 ± 0.030
20.0	0.820 ± 0.027
15.0	0.726 ± 0.035

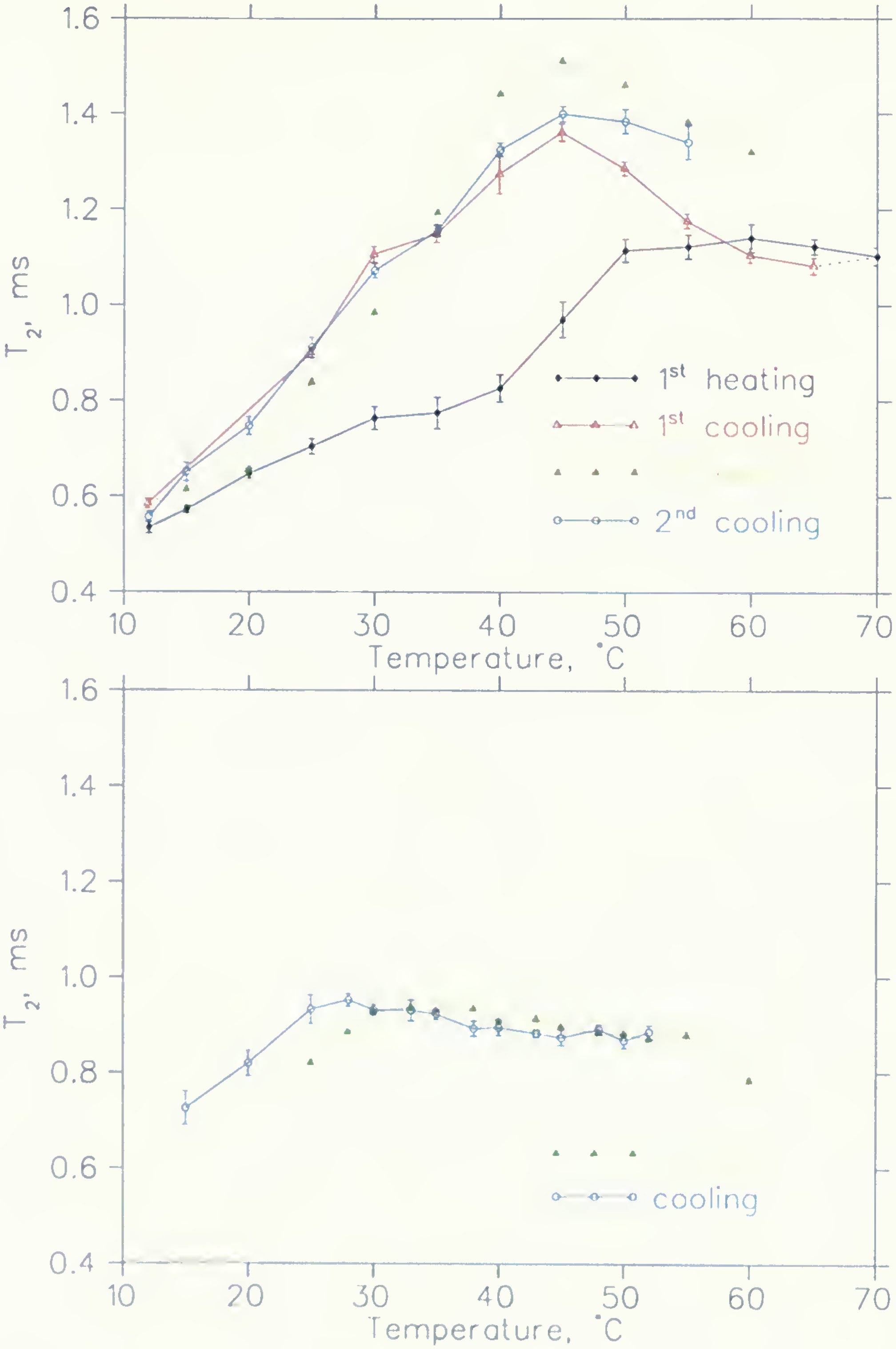

Figure 4.5: The temperature dependence of the T_2 times for the $x = 3:1$ (top) and $x = 10:1$ (bottom) samples from Tables 4.1 and 4.2.

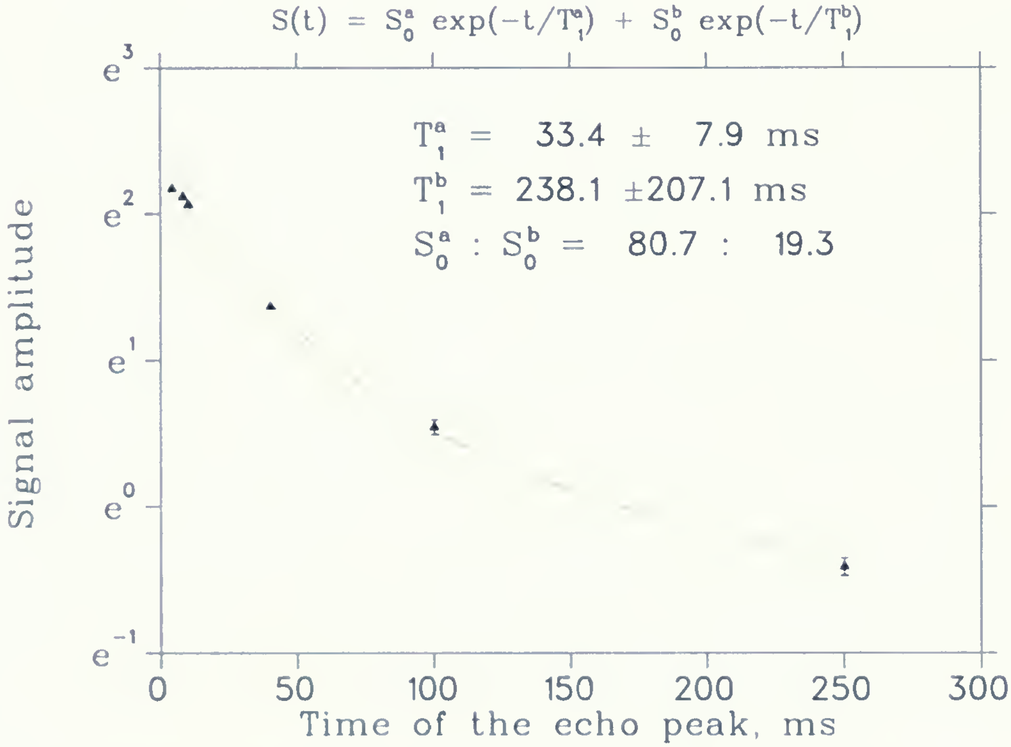

Figure 4.6: A typical fit to a two-exponential decay curve for T_{1z} times, here for the $x = 3:1$ at 25°C.

Table 4.3: T_{1z}^{ir} of the 3:1 sample

$t \pm 0.2$, °C	S_{fast}/S_{slow}	T_{1z}^{ir}fast, ms	T_{1z}^{ir}slow, ms °C	S_{fast}/S_{slow}	T_{1z}^{ir}fast, ms	T_{1z}^{ir}slow, ms
12.0	73.5/26.5	32.9 ± 6.7	225.3 ± 109.1	82.3/17.7	44.4 ± 31.3	315.2 ± 1183
15.0	69.0/31.0	21.0 ± 2.6	150.7 ± 27.5	61.2/38.8	20.0 ± 0.6	130.5 ± 3.7
20.0	75.6/24.4	22.8 ± 0.4	173.1 ± 6.2	73.0/27.0	26.6 ± 3.4	171.8 ± 43.5
25.0	74.3/25.7	24.5 ± 4.0	177.2 ± 59.8	80.7/19.3	33.4 ± 7.9	238.1 ± 207.1
30.0	76.2/23.8	27.2 ± 4.2	190.2 ± 70.1	67.4/32.6	23.6 ± 4.1	147.0 ± 36.4
35.0	81.3/18.7	32.5 ± 2.4	255.1 ± 72.4	78.9/21.1	33.7 ± 3.8	219.3 ± 77.4
40.0	75.2/24.8	30.5 ± 5.1	218.8 ± 90.6	78.5/21.5	27.9 ± 7.1	350.1 ± 322.3
45.0	70.6/29.4	32.3 ± 2.5	197.6 ± 29.1	85.9/14.1	45.5 ± 17.7	1212 ± 9673
50.0	57.9/42.1	29.1 ± 3.3	189.7 ± 22.8	67.2/32.8	33.3 ± 10.4	240.1 ± 134.9
55.0	38.0/62.0	38.9 ± 6.9	228.0 ± 59.7	53.5/46.5	25.5 ± 7.9	166.1 ± 42.4
60.0	76.5/23.5	54.9 ± 5.6	362.1 ± 165.2	82.9/17.1	54.7 ± 8.5	615.0 ± 954.2
55.0	58.8/41.2	32.4 ± 8.5	187.4 ± 55.7	57.2/42.8	37.4 ± 7.0	195.7 ± 41.5
50.0	—	—	—	64.6/35.4	31.5 ± 3.8	217.7 ± 39.2
45.0	57.6/42.4	29.0 ± 1.7	179.1 ± 10.8	71.5/28.5	33.5 ± 7.4	238.4 ± 115.6
40.0	66.7/33.3	27.0 ± 1.8	184.5 ± 18.7	69.1/30.9	26.5 ± 1.9	212.4 ± 26.8
30.0	72.3/27.7	24.3 ± 2.8	160.7 ± 34.1	76.9/23.1	29.6 ± 6.7	215.8 ± 130.9
25.0	73.0/27.0	24.4 ± 1.3	156.6 ± 15.6	76.2/23.8	28.1 ± 13.8	194.6 ± 234.5

Table 4.4: T_{1z}^{ir} of 10:1 sample

$t \pm 0.2$, °C	S_{fast}/S_{slow}	T_{1z}^{ir}fast, ms	T_{1z}^{ir}slow, ms
25.0	74.3/25.7	24.5 ± 4.0	177.2 ± 59.8
28.0	68.6/31.4	24.1 ± 0.3	206.3 ± 4.3
30.0	73.9/26.1	30.2 ± 0.6	245.8 ± 11.4
33.0	67.4/32.6	28.0 ± 7.4	212.5 ± 91.4
35.0	64.1/35.9	26.2 ± 4.4	193.0 ± 42.8
38.0	63.3/36.7	26.6 ± 7.3	200.3 ± 72.0
40.0	64.1/35.9	29.8 ± 1.8	216.1 ± 18.5
45.0	64.1/35.9	38.4 ± 2.0	243.1 ± 20.9
48.0	62.8/37.2	36.2 ± 2.9	229.0 ± 27.5
50.0	78.1/21.9	54.3 ± 8.1	434.2 ± 360.7
52.0	55.2/44.8	40.3 ± 5.3	210.4 ± 30.5
55.0	55.6/44.4	39.0 ± 9.2	218.7 ± 60.1
60.0	55.0/45.0	42.6 ± 12.1	221.5 ± 71.7
52.0	54.8/45.2	36.4 ± 8.4	211.4 ± 51.0
50.0	100.0/0.0	58.9 ± 24.9	—
48.0	67.4/32.6	44.6 ± 11.4	262.1 ± 142.5
45.0	71.4/28.6	43.7 ± 10.9	298.3 ± 202.9
43.0	90.8/ 0.0	50.6 ± 25.5	—
40.0	68.8/31.2	35.6 ± 7.5	251.9 ± 108.0
38.0	68.9/31.1	35.1 ± 1.3	242.3 ± 18.4
35.0	75.0/25.0	36.2 ± 6.0	294.7 ± 145.8
33.0	69.5/30.5	30.1 ± 3.1	225.1 ± 43.9
30.0	68.7/31.3	30.5 ± 4.0	228.3 ± 55.0
28.0	58.3/41.7	21.3 ± 1.6	138.0 ± 9.8
25.0	77.8/22.2	30.5 ± 2.3	265.2 ± 61.7

of anisotropies, $g(x)$, which is a direct measure of the order parameter profile.

The minimum of the misfit function is obtained for a slight, $(a/b)^2 = 2.0$, ellipsoidal deformation of the orientational distribution. Note the misfit is plotted at ×51 vertical scale.

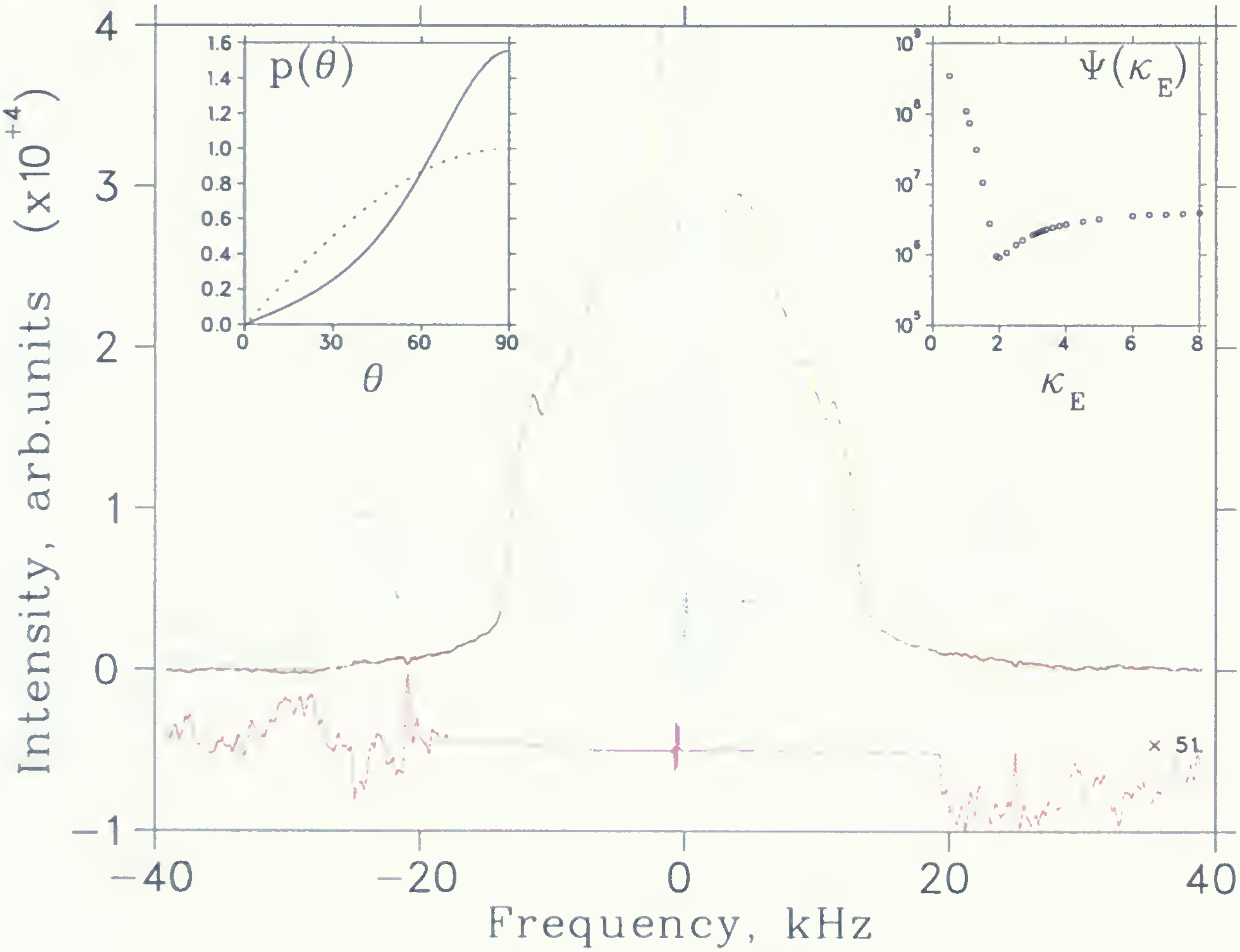

Figure 4.7: **Extracting the distribution of anisotropy from the powder spectrum of d_{54}-DMPC:Ch (10:1) sample at 35°C.** The red line is the original data and the green one is the recalculated one from the depaked $g(x)$. The misfit at the optimum value of κ_E is exceedingly small. This optimal value corresponds to a slight elliptical deformation, $(a/b)^2 = 2.0$.

As shown in Fig 4.14, the order parameter of pure DMPC is higher than that of the lipid:chlorhexidine mixture. Order parameter of the 10:1 sample follows the pattern of

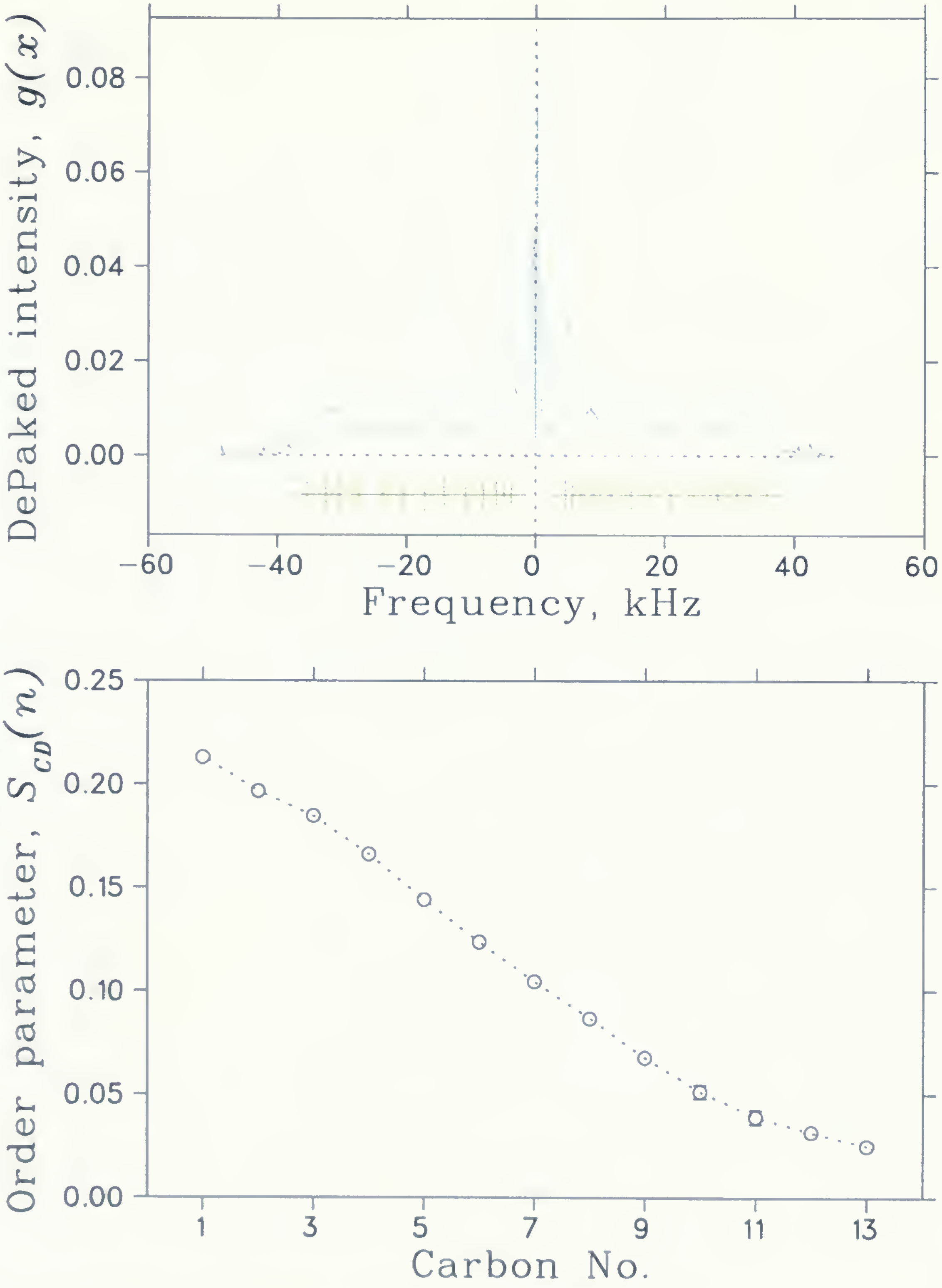

Figure 4.8: Depaked intensity and order parameter profile for 10:1 sample at 15°

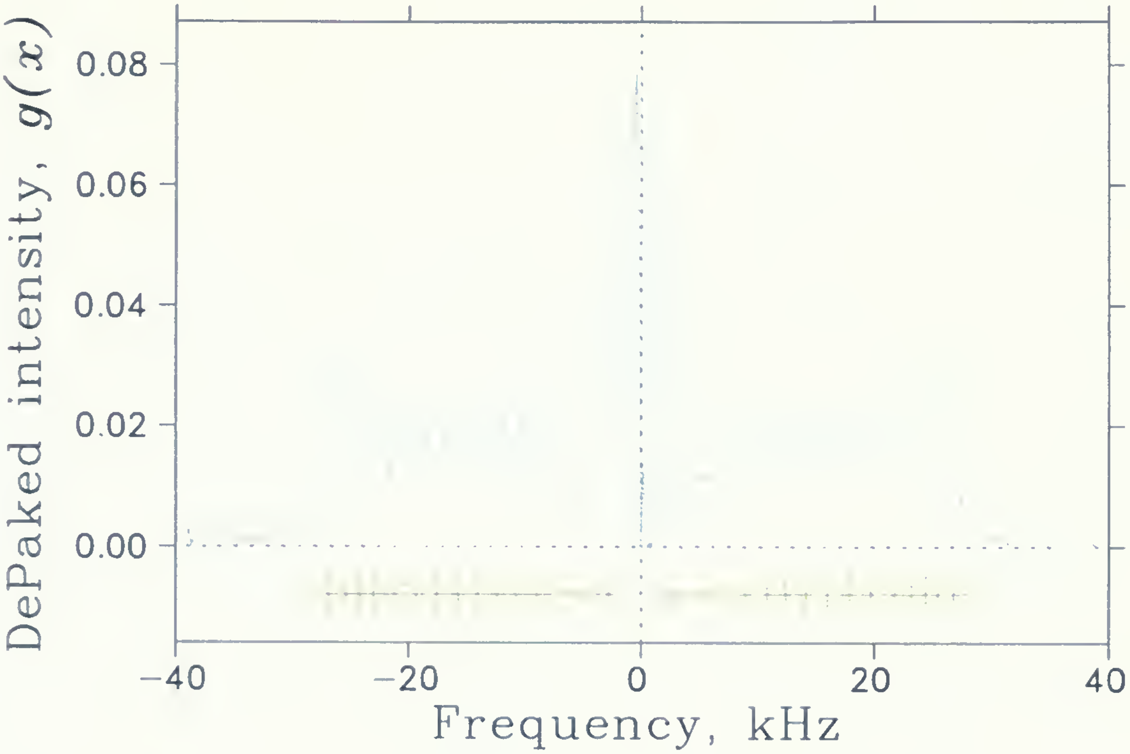

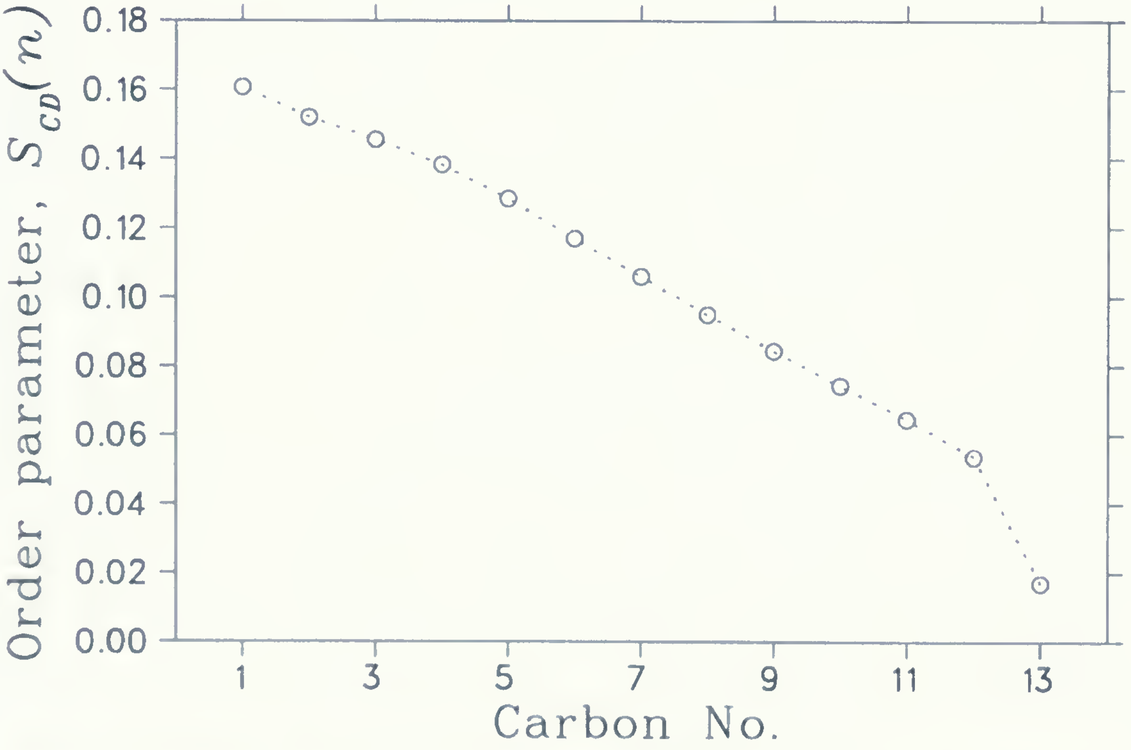

Figure 4.9: Depaked intensity and order parameter profile for 10:1 sample at 35°

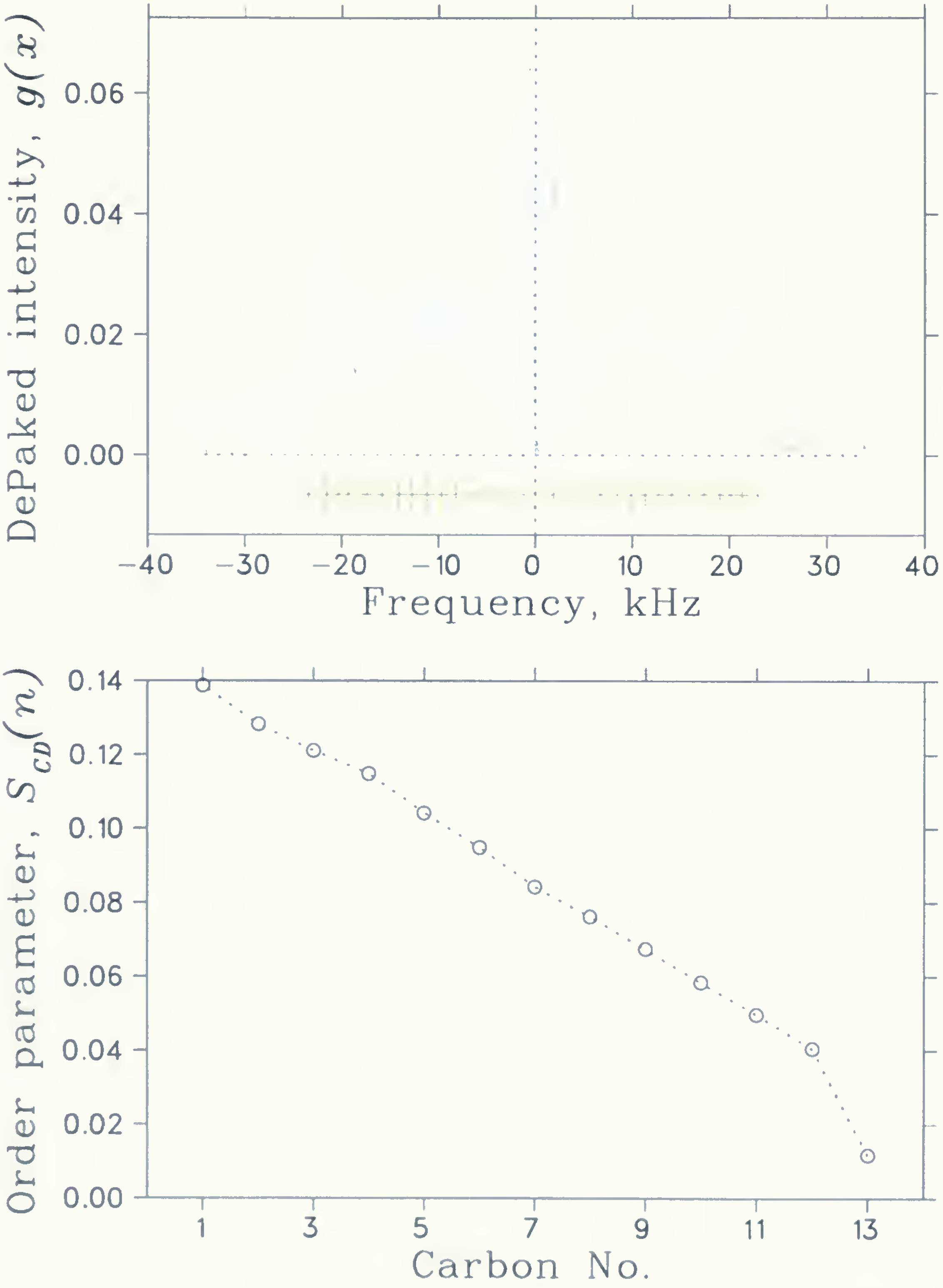

Figure 4.10: Depaked intensity and order parameter profile for 10:1 sample at 60°

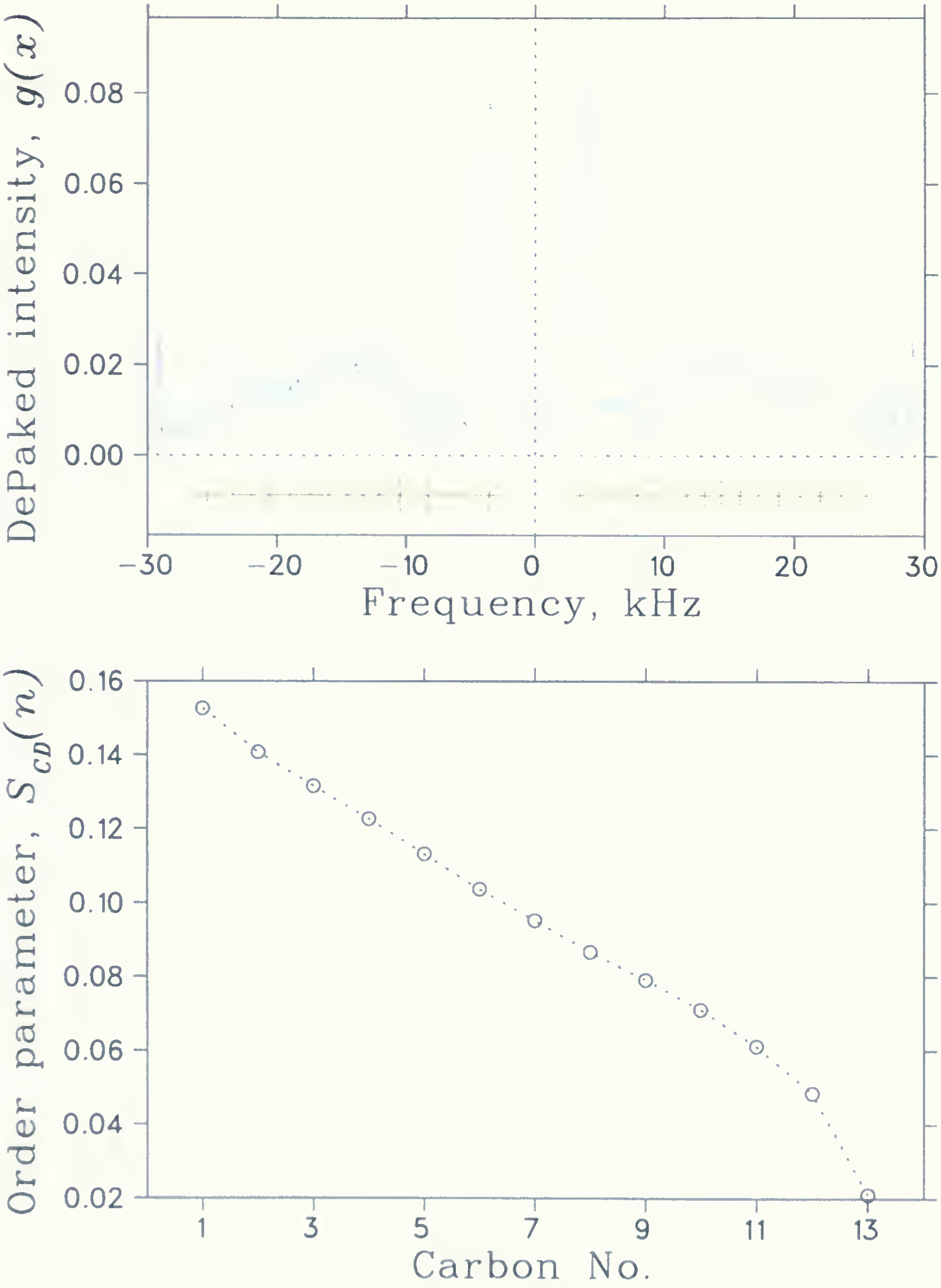

Figure 4.11: Depaked intensity and order parameter profile for 3:1 sample at 15°

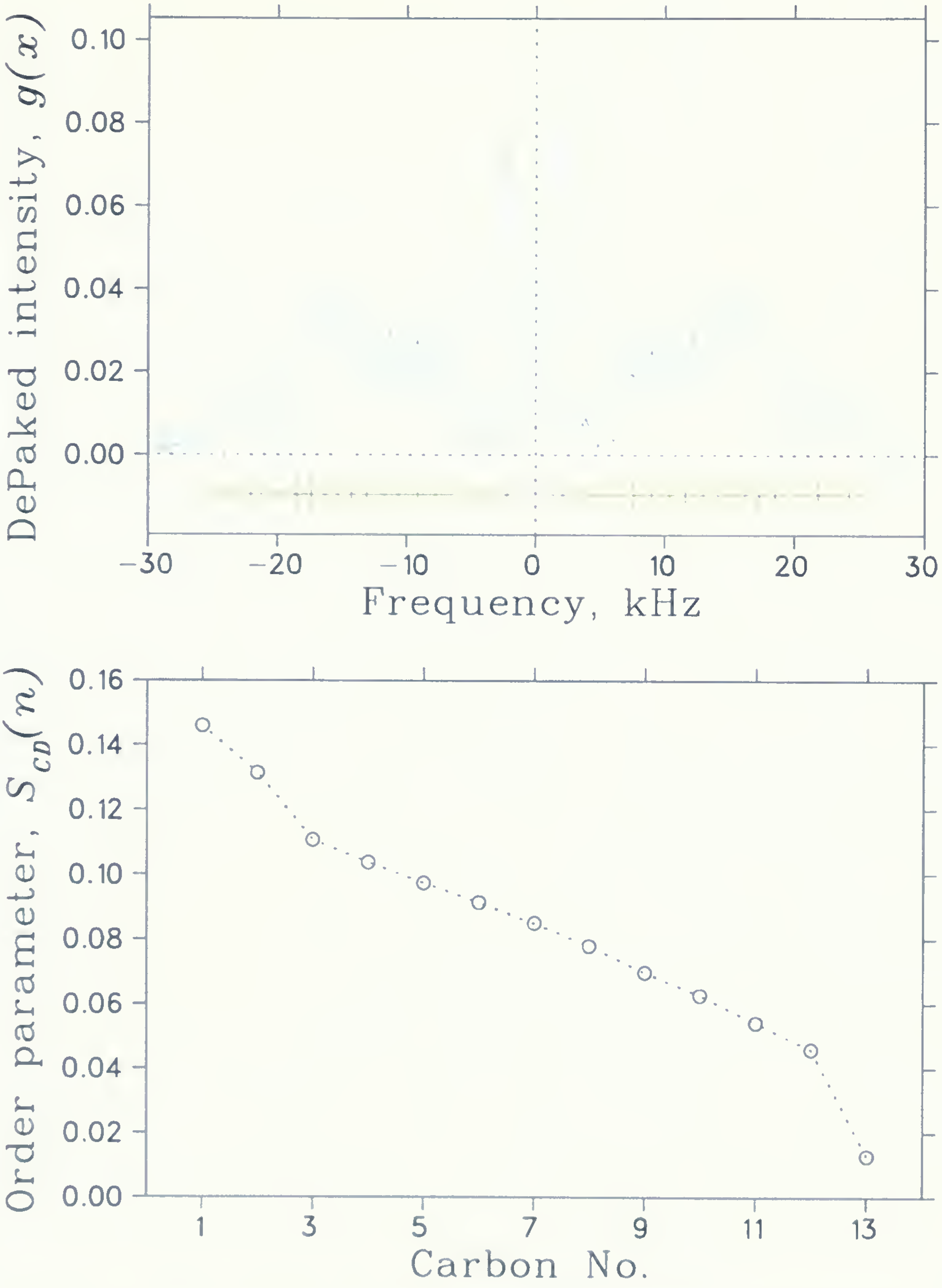

Figure 4.12: Depaked intensity and order parameter profile for 3:1 sample at 35°

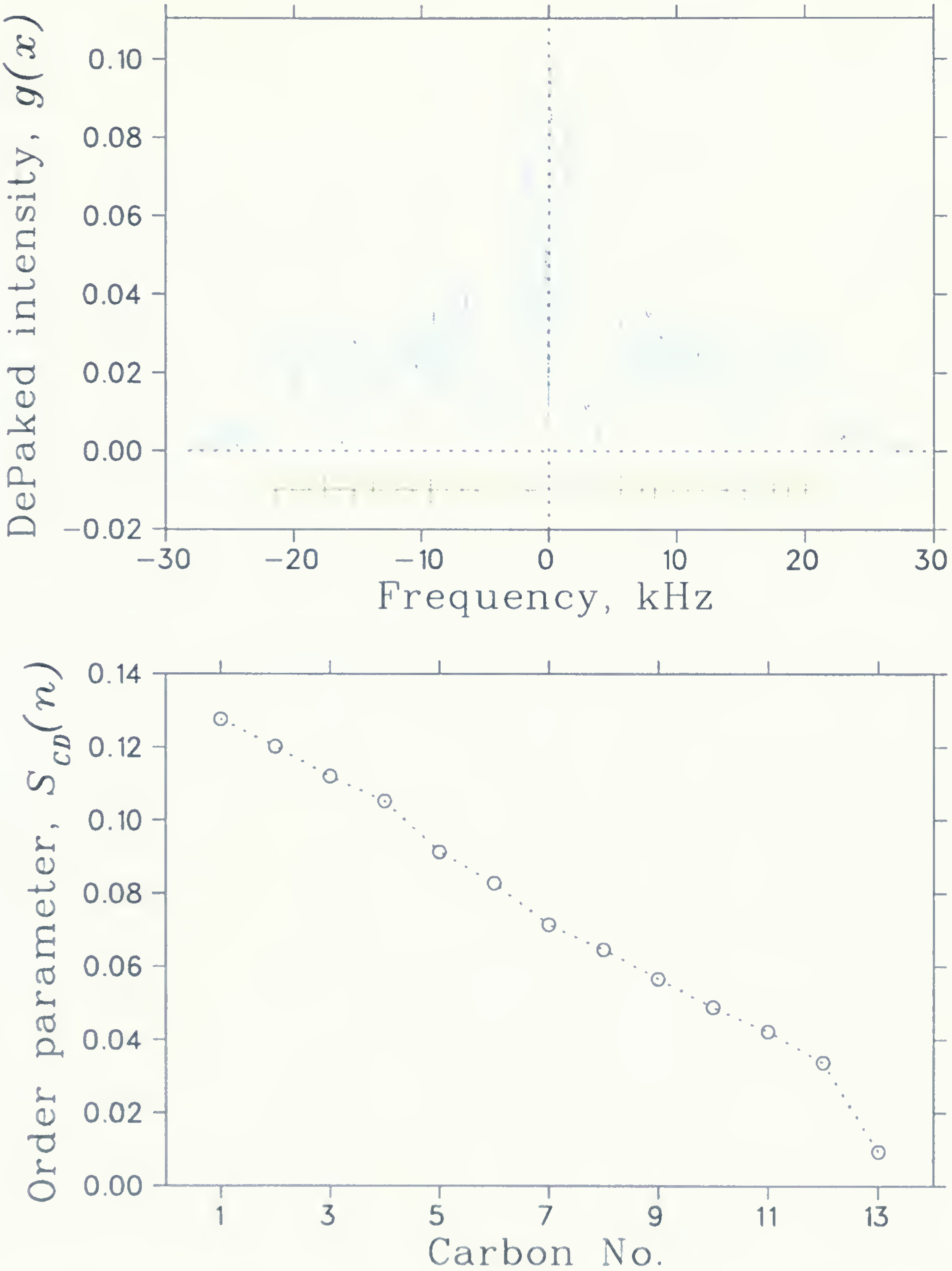

Figure 4.13: Depaked intensity and order parameter profile for 3:1 sample at 60°

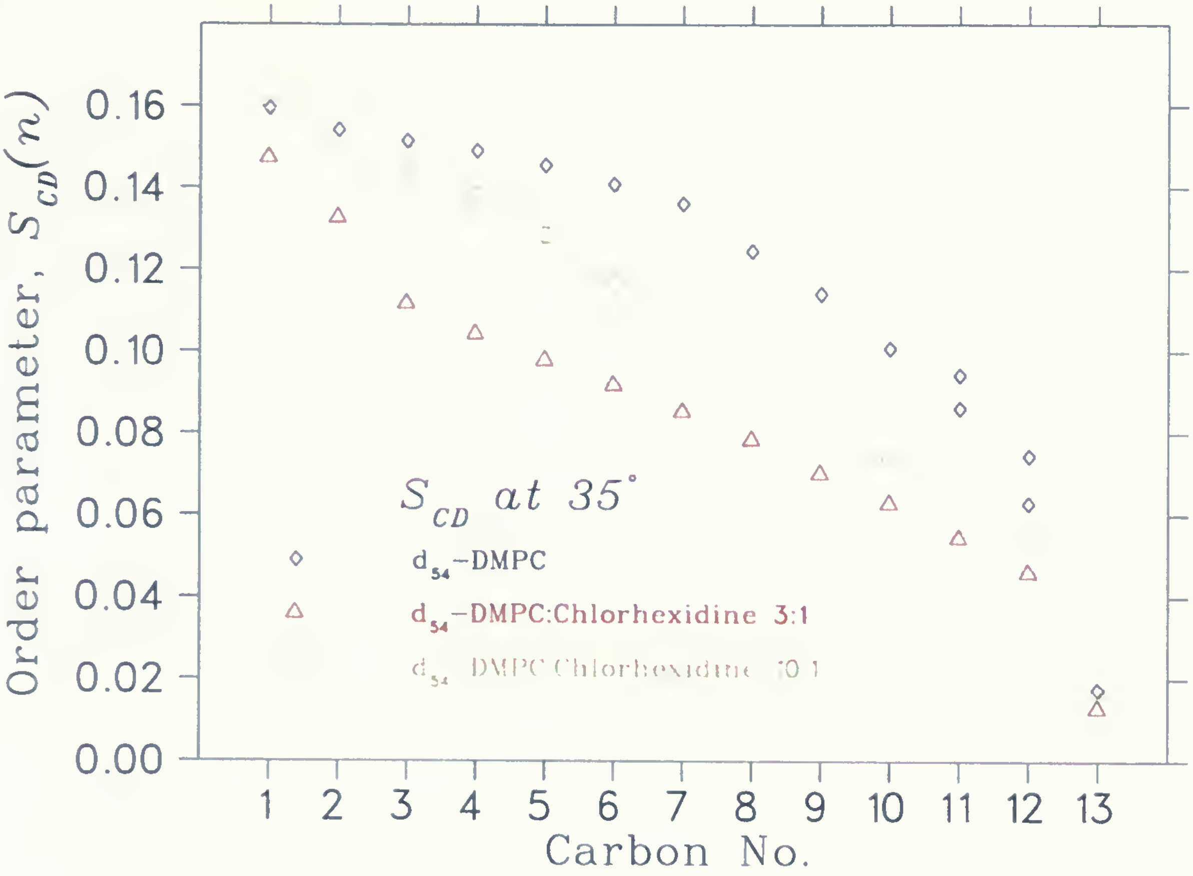

Figure 4.14: **Order parameter of pure DMPC-d54, and lipid:chlorhexidine mixtures with ratios 10:1 and 3:1** Carbon in positions 11 and 12 have two different order parameters, possibly because of their inequivalent chains. The first three carbons in pure d54-DMPC and the first two carbons in the 10:1 sample are indistiguishable. The error bars are too small to appear on the graph. The more drug in the sample, the more freedom in the lipid molecule moving axially. For the 3:1 sample, the order parameters of the first two carbons are different from the order parameters of the rest of carbons in the chain. This is a positive sign for the hypothesis that chlorhexidine is a trans-membrane drug and would then cause slow drug release.

pure DMPC-d54. Comparing order parameters of both samples at 35°C shows DMPC-d54 molecules in the 10:1 sample are more ordered than in the 3:1 sample. The more drug we have in the sample the more disordered the system becomes. In the 3:1 sample the first two carbons near the hydrophilic headgroup have less freedom to move in comparison with the other carbon atoms in the chain. This agrees with the idea that chlorhexidine molecules are trans membrane and their inner chains are located along the fatty acids of DMPC-d54.

Chapter 5

Concluding remarks

The progress made in the investigation of the properties of chlorhexidine-lipid preparations has been slower than expected and not all of the original goals have been achieved. However, a lot of valuable information about the samples has been obtained.

The properties of the samples have a complicated dependence on their thermal history. For all of the samples, the first heating cycle is different from subsequent heating/cooling cycles, as seen through the spectral lineshapes and the observed NMR relaxation rates. It also takes a long time to equilibrate these mixed samples at any temperature, even at elevated temperatures (typically this occurs anywhere within 45 min to 2 hours). This demonstrates that changes in the samples occur slowly.

In general, the spectra of the 10:1 sample looks similar to those of a pure DMPC sample, but the 3:1 sample spectra are vastly different. For both samples, the results of De-Pake-ing analysis are consistent with a mildly aligned ellipsoidal distribution of orientations at 7T, as is typical of biomembrane systems.

All of the ^{2}H NMR spectra presented here were measured in samples where the lipid molecules were labeled by isotopic substitution of hydrogen with deuterium, while the chlorhexidine remained in its protonated form. The measured order parameters for the lipid-chlorhexidine samples do not support the hypothesis of entrapment of chlorhexidine in small lipid compartments (liposomes). If small liposomes were present, the spectra would contain a narrow peak and a plateau in the order parameter. This idea has not been supported by the presented data.

T_2 relaxation time depends on bilayer shape (curvature of the bilayer) and axial motion of

phospholipid molecules. Comparison of the de-Paked intensity for the 10:1 and 3:1 samples, Fig 4.10 and Fig 4.13 respectively, show that the de-Paked intensity of the 3:1 sample is narrower than that of the 10:1 sample. It shows that phospholipids are moving faster. In the first cycle for the 3:1 sample, Fig 4.5, there is a small region of plateau between 30°C and 37°C but when the temperature is elevated, T_2 changes. It is possible before heating up the sample, that some of the drug had remained in the water, promoting low interaction between phospholipids and chlorhexidine molecules. After the sample was heated up to 60°C and kept at a constant temperature for each step of the heating process and experiment for at least two or three hours, chlorhexidine molecules were placed in the membrane.

It is possible for chlorhexidine to be found trans-membrane or found in a hexagonal phase lipid structure, but since the first two carbons have different order parameters relative to the rest of the carbons in the chain, trans-membrane location of the drug is more probable. Chlorhexidine molecules would pin down the membrane and phospholipid lateral movements would be limited by these molecules.

Chlorhexidine has two aromatic rings at both ends of the molecule and a small chain of carbons in the middle. In this hypothesis the two aromatic rings are located near the hydrophilic head of the phospholipids and in contact with water. As it is shown in the molecular model, illustrated in Fig 5.1, the first two carbons in the fatty acid chains are close to the aromatic rings and they have less freedom to move in comparison with the rest of the carbons in the fatty acid chains. As shown in Fig 4.12, the first two carbons have different order parameters. More investigations are needed using different techniques such as NOE spectroscopy [37, 17] to confirm that this hypothesis is correct.

The other model which is shown in the Fig 5.2 is also able to explain different order parameter of the first two carbons in the fatty acid chains. This second possibility is that the two rings at both ends of the chlorhexidine molecule be located near water molecules and the whole drug molecule be located towards the hydrophobic part of the phospholipids. This may suggest a hexagonal phase structure for the phospholipids. To investigate the structure of the

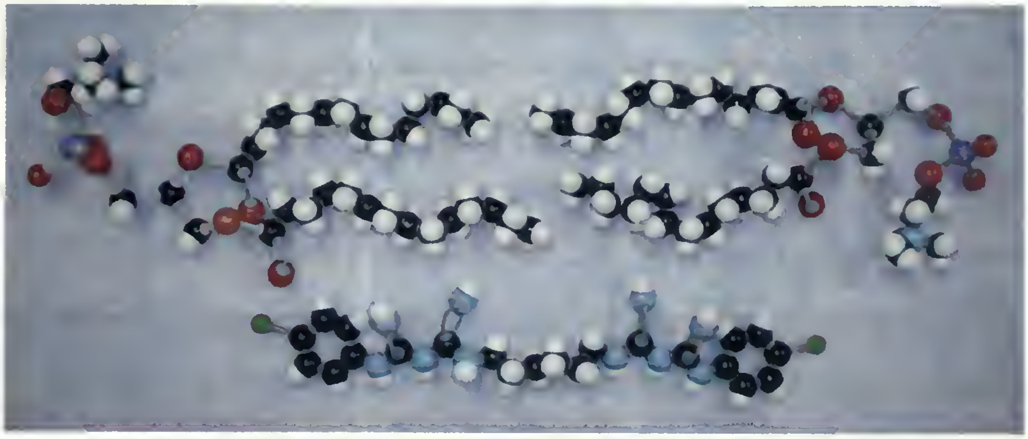

Figure 5.1: Molecular models illustrating the possibility of chlorhexidine incorporation into the DMPC bilayer

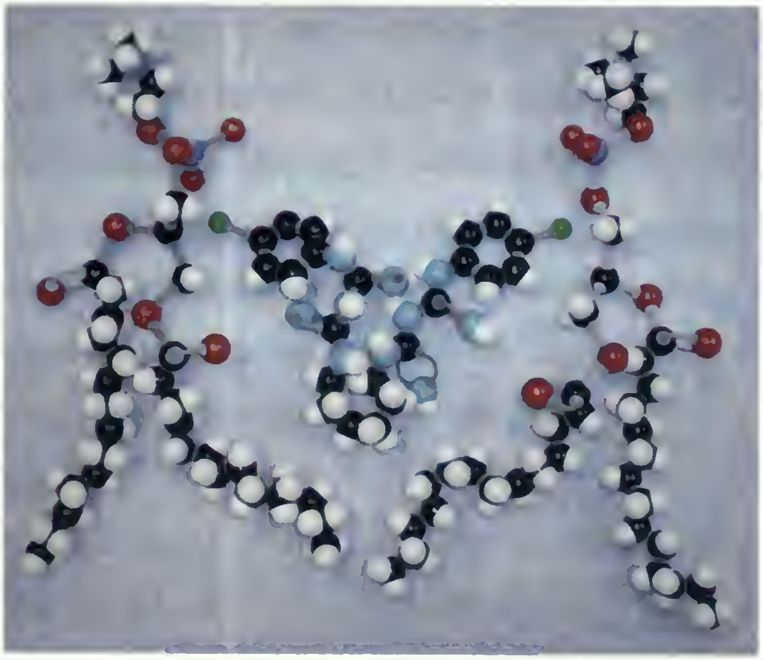

Figure 5.2: **Molecular models illustrating the aromatics of chlorhexidine located near phosphate group of DMPC.** In this model the whole chlorhexidine molecule locates in one layer of bilayer. This model explains the different order parameter of the first two carbons in the fatty acid chains. More investigation should be done from NOE [37, 17] and ^{31}P NMR.

lipid-chlorhexidine mixtures further and to determine the nature of the association between the drug and the lipid matrix, complementary measurements are needed from systems made of deuterated chlorhexidine and protonated lipid. In preparation, deuterated chlorhexidine was synthesized for the first time during this project, with an excellent yield and purity. Even though the ^{2}H NMR experiments remain to be completed, the synthesis of a new specific isotopically labeled compound represents a major achievement of this work.

The NMR experiments were delayed by technical difficulties that arose from unexpectedly low dielectric loss in the aqueous samples that led to strong and long-lived magneto-acoustic ringing in the high-Q resonance of the NMR probehead. To counteract, fairly long delay times were used in the quadrupolar echo sequence used to acquire the data, of the order of 150–180 μs. In addition, the use of standard plastic snap-closure vials sealed by a hot soldering iron proved problematic as higher than usual temperatures were explored; the samples tended to leak out above 50–60°C, and several experimental runs had to be repeated because of this. It is not clear yet how long the samples remain uniform. It is possible that some phase changes occur after keeping samples for a period of time greater than a few days. This property should be explored by other experiments to measure the changes of the size of the samples. The results shown in this work are from samples which did not leak out and whose measured weights did not change after the experiment.

Deuterated chlorhexidine is a unique and very expensive compound, and only about 100 mg of it has been synthesized successfully. Before continuing, both problems that were uncovered during this project need to be addressed: a lower-Q probehead needs to be designed and built, and a different sample vial (glass?) needs to be used that will maintain the seal at elevated temperatures. It is also crucial that the experiments be conducted in a specific order in temperature, including the initial incubation at slowly rising temperatures: we have established that reproducible results can only be obtained from samples that have undergone such an initial heating cycle.

Bibliography

[1] Theresa M. Allen. Liposomal drug formulations, rational for develpment and what we can expect for the future. *Drugs*, 56:747–756, 1998.

[2] F Bloch. Nuclear induction. *Phys. Rev.*, 70:460–474, 1946.

[3] M. Bloom, J.H. Davis, and A.L. MacKay. Direct determination of the oriented sample NMR spectrum from powder spectrum for systems with local axial symmetry. *Chem. Phys. Lett*, 80:198–202, 1981.

[4] Frank A. Bovey. *Nuclear magnetic resonance spectroscopy.* Academic Press, 1988.

[5] J. Burns. Synthesis and purification of carbon-14 labelled 1,1,-hexamethylene-*bis*-[5-(4-chlorophenyl)biguanide] (chlorhexidine, 'hibitane'). *J. Labelled Compounds and Radiopharmaceuticals*, 19:1239–1250, 1982.

[6] Richard Hermann Cleve. Role of 10- and 14-carbon alkanes in HII phase of DOPE. Master's thesis, Brock University, 1998.

[7] G.E. Davies, J. Francis, A.R. Martin, F.L. Rose, and G. Swain. 1:6-di-4-chlorophenyldiguanidohexane ('hibitane'). Laboratory investigation of a new antibacterial agent of high potency. *Brit. J. Pharmacol.*, 9:192–196, 1954.

[8] J. H. Davis, K. R. Jeffrey, M. Bloom, M. I. Valic, and T. P. Higgs. Quadrupolar echo deuteron magnetic resonance spectroscopy in ordered hydrocarbon chains. *Chem. Phys. Lett.*, 42:390–394, 1976.

[9] J.H. Davis. The description of membrane lipid conformation, order and dynamics by 2H-NMR. *Biochim. Biophys. Acta.*, 737:117–171, 1983.

[10] J.H. Davis. Deuterium nuclear magnetic resonance spectroscopy in partially ordered systems. *Isotopes in the Physical and Biomedical Sciences*, pages 99–157, 1991.

[11] Claus O.Meeseand Otto Fürst and Bernd Borstel. Dimethyl 3,3,4,4,5,5,6,6-($^2H_8$)-6-methoxycarbonyl-2-oxo-hexanephosphonate, a versatile reagent for the synthesis of deuterated ω-carboxy prostanoids. *J. Labelled Compounds and Radiopharmaceuticals*, 23:175–185, 1986.

[12] Robert B. Gennis. *Biomembranes Molecular Structure and Function*. Springer-Verlag, 1989.

[13] Rust H. Characterisation of DMPC/DHPC mixtures by ^{31}P and ^2H solid-state nmr, 1998.

[14] Helmut Heller, Michael Schaefer, and Klaus Schulten. Molecular dynamics simulation of a bilayer of 200 lipids in the gel and in the liquid-crystal phases. *J. Phys. Chem.*, 97:8343–8360, 1993.

[15] T. D. Hennessey. Some antibacterial properties of chlorhexidine. *J. periodont. Res.*, 8:61–67, 1973.

[16] J. Honerkamp and J. Weese. Tikhonov's regularization method for ill-posed problems. A comparison of different methods for the determination of the regularization parameter. *Contin. Mech. Thermodyn.*, 2:17–30, 1990.

[17] D. Huster and Gawrisch. Noesy nmr crosspeaks between lipid headgroups and hydrocarbon chains: Spin diffusion or molecular disorder? *J. Am. Chem.*, 121:1992–1993, 1999.

[18] R. Lipowsky, D. Richter, and K. Kremer. Molecular structure of membranes. In K. Kremer R. Lipowsky, D. Richter, editor, *The structure and Conformation of Amphiphilic Membranes*. Springer-Verlag Berlin, 1991.

[19] Harold Lõe and C. Rindom Schiøtt. The effect of mouthrinses and topical application of chlorhexidine on the development of dental plaque and gingivitis in man. *J. Periodont. Res.*, 5:79–83, 1970.

[20] A. Matsaev, L. Lurya, and E. Lurya. Antimicrobial oral rinse: Controlled release, lipid based delivery formulation of chlorhexidine (lbd-chx), a pilot study in healthy subjects. Technical report, Lurident Ltd., Derech Hatasiya 70/2, Kiryat Gat 82000, Israel, 1997.

[21] O.G. Mouritsen, J. H. Ipsen, K. Jrgensen, M. M. Sperotto, Z. Zhang, E. Corvera, D. P. Fraser, and M. J. Zuckermann. Computer simulation of phase transitions in nature's preferred liquid crystal: the lipid bilayer membrane. In G. F. Luckhurst, editor, *Computer Simulation of Liquid Crystals*. Kluwer Academic Publishers, Dordrecht, The Netherlands, 1992.

[22] Marc J. Ostro and Pieter R. Cullis. Use of liposomes as injectable-drug delivery systems. *American Journal of Hospital Pharmacy*, 46:1576–1587, 1989.

[23] G.E. Pake. Nuclear resonance absorption in hydrated crystals: Fine structure of the proton line. *J. Chem. Phys.*, 16:327–336, 1948.

[24] M. Rance and R. A. Byrd. Obtaining high–fidelity spin–1/2 powder spectra in anisotropic media: Phase–cycled Hahn echo spectroscopy. *J. Magn. Reson.*, 52:221–240, 1983.

[25] R.Machinek and W.Lüttke. A convenient preparation of $^2H_8$-dibromoalkynes from alkynediols. *Synthesis*, pages 255–256, 1975.

[26] F.L. Rose and G. Swain. Bisdiguanides having antibacterial activity. *J. Chem Soc.*, pages 4422–4425, 1956.

[27] H. Schäfer, B. Mädler, and E. Sternin. Determination of orientational order parameters from ^{2}H NMR spectra of magnetically partially oriented lipid bilayers. *Biophys. J.*, 74:1007–1014, 1998.

[28] H. Schäfer and R. Stannarius. Calculation of orientational distributions of partially ordered samples from NMR spectra. *J. Magn. Reson. B*, 106:14–23, 1995.

[29] H. Schäfer and E. Sternin. Inverse ill-posed problems in experimental data analysis in physics. *Physics in Canada*, 53:77–85, 1997.

[30] Carsten Schmuck and Micheal Schwegmann. A molecular flytrap for the selective binding of citrate and other tricarboxylates in water. *J.Am.Chem.Soc.*, pages 3373–3379, 2005.

[31] Charles P Slichter. *Principle of magnetic resonance.* Springer, 1996.

[32] Frank L. Sorgi and Leaf Huang. Drug delivery applications. *Current Topics in Membrane*, 44:449–475, 1998.

[33] E. Sternin. *Some Mechanisms of Transverse Nuclear Magnetic Relaxation in Model Membranes.* PhD thesis, University of British Columbia, 1988.

[34] E. Sternin. RF phase shifting at the source simplifies NMR spectrometer design. *Rev. Sci. Instrum.*, 66:3144–3145, 1995.

[35] E. Sternin. **dans** — Data Analysis of NMR Spectra. Available at http://www.physics.brocku.ca/faculty/sternin.html, 1999.

[36] E. Sternin, M. Bloom, and A. L. MacKay. De-Pake-ing of NMR spectra. *J. Magn. Reson.*, 55:274–282, 1983.

[37] E. Sternin, D. Nizza, and K. Gawrisch. Temperature dependence of DMPC/DHPC mixing in bicelles and its structural implications. *Langmuir*, 17:2610–2616, 2001.

[38] E. Sternin, H. Schäfer, I. Polozov, and K. Gawrisch. Simultaneous determination of orientational and order parameter distributions from NMR spectra of partially oriented model membranes. *J. Magn. Reson.*, 149:110–113, 2001.

[39] Robin L. Thurmond and Göran Lindblom. Nmr studies of membrane lipid properties. *Current Topics in Membrane*, 44:103–168, 1998.

[40] Zuzana Trskova. Nmr characterization of chlorhexidine in lipid based formulations. Master's thesis, Brock University, 2004.

[41] Monique H. Vingerhoeds, Gert Storm, and Daan J. A. Crommelin. Immunoliposomes in vivo. *Immunomethods*, 4:259–272, 1994.